Microstructural and Mechanical Property Characterization of Laser Additive Manufactured (LAM) Rhenium

by

Robbie Adams

A Dissertation Presented in Partial Fulfillment
of the Requirements for the Degree
Doctor of Philosophy

Approved April 2012 by the
Graduate Supervisory Committee:

Nikhilesh Chawla, Chair
James Adams
Stephen Krause

ARIZONA STATE UNIVERSITY

May 2012

ABSTRACT

This report will review the mechanical and microstructural properties of the refractory element rhenium (Re) deposited using Laser Additive Manufacturing (LAM). With useable structural strength over 2200 °C, existing applications up to 2760 °C, very high strength, ductility and chemical resistance, interest in Re is understandable. This study includes data about tensile properties, fatigue and microstructure including deformation systems and potential applications of that information. The bulk mechanical test data will be correlated with nanoindentation and crystallographic examination. LAM properties are compared to the existing properties found in the literature for other manufacturing processes. The literature indicates that Re has three significant slip systems but also twins as part of its deformation mechanisms. While it follows the hcp metal characteristics for deformation, it has interesting and valuable extremes such as high work hardening, potentially high strength, excellent wear resistance and superior elevated temperature strength. These characteristics are discussed in detail.

ACKNOWLEDGMENTS

I would like to thank Prof. Nikhilesh Chawla for his guidance and assistance with this research. The following past and present group members provided assistance: Jason Williams and Ling Jiang of the ASU Mechanical Laboratory, Grant Crawford, Martha Dudek, Danny Singh, Xin Deng, Kyle Yazzi, Eric Padilla and Nick Chapman. I would also like to thank the Honeywell management for funding a portion of this research and the following Honeywell Materials Laboratory staff: Mr. Jim Hartman, Mr. Russ Bartos, Mr. Don Benjamin and Mrs. Diana Chapa. Dr. ZhenQuan Liu of the ASU Center for Solid State Materials provided significant assistance with microscopy. I would like to acknowledge the assistance of AeroMet Corporation for early funding and Mr. Frank Arcella of AeroMet for guidance and support in this project. Mr. Todd Leonhardt of Rhenium Alloys Inc. (RAI) also provided guidance. Also, RAI provided raw material to AeroMet. Initial ultra-high tensile testing was performed at Southern Research Institute (SORI) in Birmingham AL and early scanning electron micrcroscopy was performed at the University of AL Birmingham under the direction of SORI. Finally I would like to thank my family for their support in this endeavor.

TABLE OF CONTENTS

LIST OF TABLES

LIST OF FIGURES

1. INTRODUCTION

Rhenium (Re) is a refractory metal with many attractive properties and valuable commercial uses but with manufacturing and availability challenges.[1-7] It is classified as a refractory because it has a melting point of 3180 °C.[1] About 70 percent of Re is used as an alloying element in super alloys to maintain strength at jet engine operating temperatures.[8] Oil refineries employ another 20 percent as a catalyst in combination with platinum.[1, 4, 7, 8] The combined uses account for approximately 90 percent of Re production.[8] Other applications include use in ultra-high temperature rockets and heavy wear and/or arc erosion electrical switch components, thermocouples. Alloying rhenium with tungsten and molybdenum significantly increases the ductility of both materials at room temperature.[7] The optimum combination of strength and ductility occurs with 20 to 30 percent of Re alloyed with tungsten and 40 to 50 percent alloyed with molybdenum.[6]

Knowledge of Re begins with Walter and Ida Noddack (Tacke) and O. Berg when they discovered it in 1925 in Germany.[4] It was the last natural element found. Re is a byproduct of copper and molybdenum mining and its ore is produced in Arizona, Germany, Siberia, South America and other locations.[4, 8] Re metal is produced from several processes and one commonly used process is extraction from molybdenum ore. Molybdenum flue dust containing rhenium is oxidized, trapped in a filter then liquefied in an aqueous solution, mixed with potassium chloride, and neutralized with ammonium hydroxide. Ammonium perrhenate (NH_4ReO_4) is precipitated from the resultant solution.[1, 4] The precipitate is then converted to pure rhenium metal in a hydrogen atmosphere.[4, 7]

Re has mechanical properties that are attractive compared to other elevated temperature materials.[1, 4, 7, 9, 10] Unlike some refractory metals such as tungsten and

molybdenum, Re is ductile at room and cryogenic temperatures having no brittle-to-ductile transition temperature.[1, 4] Yet between room temperature and 1200°C, Re has twice the strength of tungsten.[1] In the annealed state at room temperature (RT), Re has strength and ductility analogous to 300 series stainless steels (SS). Many SS have an ultimate tensile strength (UTS) to yield strength (YS) ratio of approximately two and an elongation ranging from 30 to 50 percent. Annealed Re UTS to YS ratio is approximately 3 and elongation of conventionally produced Re at room temperature has been reported as higher than 30 percent.[1, 4, 7] Such a spread can be indicative of high ductility but also high work hardenability. In fact rhenium Re work hardens at a very high rate with a strain-hardening exponent of 0.353.[1, 4, 7] The ductility combined with high hardenability allows it to be worked to a UTS of over 2 GPa.[1, 4, 7]. It also has a high elastic modulus typically reported as 460 GPa.[1, 4, 7] That is much higher than steel with a modulus of 206 GPa. Another of its outstanding mechanical properties is useable strength in neutral or reducing atmospheres approaching its melting point i.e. a strength of 48 MPa at 2204 °C.[10] Some other commercial alloys would be liquid at these temperatures.

Surprisingly, since it is very ductile, Re resists wear effectively.[1, 2, 4, 7, 11, 12] Normally ductile materials are not wear resistant. Re is also very resistant to chemical attack in many environments including sulfuric and hydrochloric acid[1, 4, 7] and it is highly resistant to seawater attack.[1, 4] In neutral or reducing environments Re has been shown to be highly erosion resistant to arcs.[4, 7] However, it is readily dissolved by oxidizing acids such as nitric.[4, 7]

Unfortunately, Re is not oxidation resistant. The pure metal oxidizes at low temperature and produces a volatile oxide, rhenium heptoxide, Re_2O_7, at approximately 360 °C.[1, 4, 7] At higher temperatures in oxidizing environments, it may oxidize

catastrophically. Re alloys that are resistant to oxidation at the low portion of the useful elevated temperature ranges have been created but are not the subject of this study.

These excellent combinations of properties result from its electronic structure. Re is a member of the Group VII B in the sixth period of the periodic table and is part of the group considered transition metals.[1, 4] It has an atomic number of 75 with a valence state between +7 and –1. Its atomic weight is approximately 186.3 and a theoretical density of 21.0 g/cm.[1, 4, 7] Re has a hexagonally close packed (hcp) structure and behaves like many other hcp materials but has trends of its own. Its c/a ratio of 1.616 is less than the ideal (1.63) for close packing.[4] The lattice constants are a = 2.75 A, C = 4.46 A.[4, 5, 6]

While Re has many attractive properties, it unfortunately has four major drawbacks: Cost, availability, manufacturability and poor oxidation resistance.[1, 4, 7] The material is expensive with limited availability. In addition to low availability, the cost, at least in part, is due to the high usage in alloys as solid solution strengthener and as a catalyst in oil refineries. Part of the poor manufacturability of Re is its propensity to crack during formation with deformations in excess of approximately 10 percent. The high melting point makes casting impractical and high strength at elevated temperatures makes forging difficult. In addition, the propensity to crack even at elevated temperature complicates hot working even more and makes it quite costly as frequent annealing steps are required. Finally the high rate of work hardening makes single point turning impractical. Re can be ground but that is very slow and only cost effective for removal of small amounts of material such as that found in high tolerance surfaces.

Currently Re stock is manufactured commercially using 1. powder metallurgy (PM) 2. PM hot isostatically pressed (PM HIPed) ingot, 3. PM cold rolled plate (PM CR)

and 4. chemical vapor deposition (CVD) thin walled structures.[1, 3, 4, 7] Individual components and their features are fabricated by use of electro discharge machining and diffusion bonding. Several newer processes are getting increased scrutiny including 1.Salt bath electro-deposition[13] 2.spray forming[14] 3. electron beam-physical vapor deposition (EB-PVD)[15, 16] and 4. additive manufacturing (AM).[17, 18, 19] These new processes are being developed to overcome some of the disadvantages of the older approaches. However each of these processes has their own characteristics that influence their mechanical properties and their ability to be formed into useable shapes. The formability characteristics and mechanical properties can be attributed to the microstructure and dislocation behavior of the type of Re used. All these various methods produce different microstructure which results in different properties.

One of the newer approaches that can mitigate these fabrication problems is additive manufacturing (AM). AM uses only the material needed by making near net shape components, thus material costs due to scrap can be reduced if not eliminated. Alternatively, AM can apply Re as a coating and still provide the utility of its properties. Thus, the total expenditure for very expensive Re per component could be reduced. Many AM processes exist today but the appropriate AM system can easily manufacture Re parts otherwise difficult to fabricate.

Before commercial advantage can be taken of the benefit of AM deposited Re, additional technical information is required. Very little has been found in the literature describing the microstructure of AM deposited Re or the influence the microstructure, including crystallographic orientation, has on mechanical properties. Furthermore there is a dearth of information in the public literature about the ultra-high temperature mechanical properties of Re. Define ultra-high temperature as $\geq$ 1648 °C. Many of the

rocket structural applications operate in this temperature regime. Limited information regarding testing thin layers of Re and correlation with bulk properties is available in the literature.

This report reviews Re properties and this research evaluating deposits from one type of AM Re depositing process called Laser Additive Manufacturing (LAM). LAM is a laser based type of additive manufacturing. This report presents data from studies of microstructure with electron backscattered diffraction (EBSD), nanoindentation testing, tensile testing, fatigue and electron microscopy examination.

2. LITERATURE REVIEW

Processing

Lack of practical viability for conventional fabrication methods like single point turning, casting and grinding have led to the development of the processes listed previously each with different properties.[13-29] Every process has very different deposition and consolidation mechanisms. Different deposition processes and parameters often lead to different grain morphology and size. The formability and mechanical properties characteristic of each process can be attributed to the microstructure and resulting deformation behavior of the type of Re used. Currently the majority of Re shapes are produced using powder metallurgy (PM) techniques and chemical vapor deposition but other processes are making inroads.

Powder metallurgy consolidation is carried out at very high temperature and pressure. In one PM procedure, noted by Koeppel and Subhash[29], Re powder was loaded into a container and subjected to high pressure at, 415 MPa, at room temperature. Then it was pre-sintered at 1200°C followed by a final sinter at 2700 °C in vacuum or hydrogen atmosphere. It can be worked further and often is until 99 percent density is achieved. Often PM ingots are porous, usually containing microporosity, and the porosity can vary throughout the shape.[27, 30] It may not be visible to the naked eye but further processing, such as welding, may consolidate to unacceptably large pores.[30] Also at ultra-high temperatures, above 1648 °C, the material can have low ductility of 5 percent or less.[31, 32] Re may be sold commercially in powder form or it may be sold processed even further into other forms like plate and other shapes.

Wrought shapes such as rolled sheet, plate and drawn or forged rod start as a powder. It is then consolidated as noted above and then shaped into a wrought form by

further application of force at elevated temperatures.[1, 4, 7] It is noted here as a separate form, since it undergoes an additional working step and is treated as such in the literature. One of the advantages of plate, in addition to its form, is lower porosity.

Chemical vapor deposition (CVD) of rhenium results when rhenium, which has been chemically combined with a halogen such as chlorine or fluorine, is subjected to heat in the presence of a substrate and pure Re is depsited.[3, 24] The grains grow perpendicular to the surface of deposition and the strength is directional. Parallel to the axis of the grains, the material is very strong but transverse to the columnar grain the strength is lower as is ductility. Chlorine CVD rhenium typically has low bend ductility. Its value lies in its ability to apply thin coatings especially on a contoured surface.

Rhenium can be deposited electrolytically. One commercial process used to deposit Re electrolytically is called El-Form™ employed by Plasma Processes, Inc.[13] The process deposits refractory metals in an elevated temperature molten salt bath covered by an inert atmosphere to protect materials sensitive to oxygen. Their process is capable of producing high purity deposits. The deposit thickness can range from microns up to millimeters.[13]

Another process attracting attention is spray forming. The process sprays molten metal onto a mandrel that has the desired shape. The mandrel is then removed. It is a near-net-shape process and produces dense deposits.[14]

Electron Beam Physical Vapor Deposition (EB-PVD) Re[15, 16] focuses an electron beam on the Re starting source. Material is vaporized and then condenses on a suitable target.

Additive manufacturing (AM) is a process in which a part is built in three dimensional space and requires no molds, mandrels or patterns.[17, 18, 19] A computer and program replaces the molds, mandrels and patterns by directing deposition of small amounts of molten metal until a shape is built. Laser Additive Manufacturing (LAM) is one type distinguished by its use of a laser as a heat source. It fits into the category of direct metal deposition (DMD).

AM processes are numerous but they have common characteristics that assist in solving some of the conventional fabrication processes disadvantages like casting, single point turning, grinding and forming.[17, 18, 19] The majority of the AM processes deposit in layers. The thickness of the layers varies with AM type. As one might expect the deposit size varies with heat input and feedstock feed rate. By building in layers with only incremental melting, a large variety of shapes can be built. One way to think about these processes is as a computer controlled casting where the shape itself acts as a mold for the small amounts of material to be deposited. This approach enables the heat input to match the feedstock rate. Thus for a material like Re with its high melting point, the heat is matched to the amount of material fed to the deposition point per unit time and it is easily fused. The Re starting plate, and the subsequent deposits, act as its own mold. This solves the problem of conventional casting in that the mold materials can easily withstand the high melting point of the feedstock. Since the process is near net shape, the amount of machining after deposition can be significantly reduced and the amount of Re scrap can be reduced. Finally, since no forming is involved and Re is very ductile, the likelihood of cracking is significantly reduced, if not eliminated.

AM Re discussion in the literature is very limited in contrast to bulk Re studies. The latter define many properties of bulk Re well. Only one presentation about AM Re

has been found to date. It is informative but much more information is needed to characterize the material and take advantage of the process. The material available from that study will be discussed in the next two sections.

It must be noted that Re mechanical properties, including LAM, are influenced by multiple parameters including grain size, grain morphology, deformation mechanisms oxygen content, other impurity contaminants, etc.

Rhenium Microstructure

Define microstructure as those constituents within a metal that are sufficiently small as to require magnification to be seen. Typically this is thought of as grain size and morphology, second phases, twins, slip lines, etc. that can be seen using optical microscopy. However some features such as precipitates, which are a second phase, are sometimes so small that microscopy of other types that magnify higher than that available from optical instruments is required. In addition to second phase precipitates, include internal features such as crystal orientation, dislocations, dislocation clusters, etc. Re grain morphology and crystal orientation can be heavily dependent on manufacturing process.

Powder metallurgy produced forms such as ingots, rods, etc. that have been sintered or hot isostatically pressed have equiaxed grains.[27, 30, 31] Chlorine CVD deposits have columnar grain deposits and directed perpendicular to the surface.[3] Fluorine based Re CVD has more equiaxed grains but can have higher porosity.[24] In salt bath electro-deposited rhenium, El-Form, grains are columnar as-deposited but equiaxed after annealing. The porosity is low but ductility is high.[13] EB-PVD and Spray Formed Re

produces fine equiaxed grains[14] on the order of 5 to 7 microns as contrasted to CVD which can have grains over ten times that size.[15, 16]

Arcella et al.[17, 18] in two separate publications presented results about LAM Re deposits. They found the grains to be large, equiaxed and varied in grain size. They only checked the view perpendicular to the build direction in the first study[17] and added a view parallel to the build direction in the second study.[18] The latter image presented in that study also appeared equiaxed but irregular.

These studies were the only ones found describing either LAM Re or any AM deposited Re. Gaps in the fundamental understanding of LAM Re microstructure consist of a full study of the orthogonal views of LAM Re microstructures as well as the crystallographic orientation of those grains. In addition, no studies have been published investigating whether any crystallographic preferred orientation exist. Finally no deformation studies have been undertaken for LAM Re.

Dislocation Systems in Rhenium

Most of the Re structural applications of interest use polycrystalline materials. Churchman[9] published one of the earliest comprehensive studies of Re deformation behavior. He studied polycrystalline materials and found that slip occurs on the (0001) and $\{10\bar{1}0\}$ and to a lesser extent slip occurs on $\{10\bar{1}1\}$ planes. He suggested that Re strengthening depends on dislocation interactions connected to $\{10\bar{1}0\}$ systems. See Table 1. Other findings by Churchman included kink bands observed simultaneously with $\{10\bar{1}0\}$ slip. Distortion in one grain can be accommodated by distortion in an adjacent grain if that grain is oriented such that it has a slip system parallel to the grain boundary. However if one grain significantly distorts more than its neighbor does, this non-uniform

distortion can lead to grain boundary dislocation pileups and microcracking and ultimately visible cracking at the surface.[33] This results in brittle fracture and often the fracture mode is intergranular.[33, 34] In fact the predominate mode for Re fracture at room temperature is intergranular fracture.[4, 9, 31, 32] As noted earlier, the ductility at RT is often high. This seeming contradiction may be explained by the need to have 5 independent slip systems to enable deformations of polycrystalline materials.[35] Re does not meet that criterion since it has an hcp crystal structure and has 3 dominate slip systems.[9, 36, 37] See Table 1. If on the other hand, a slip system is oriented parallel to the grain boundary the distortion is accommodated by the system.[9] If no systems are parallel to the boundary, then cracking can result.[9]

Finally Churchman[9] suggested that the high rate of work hardening may be due to intersecting prismatic slip dislocations. To elaborate, he contended the stacking fault energy in Re was low and that could lead to greater separation of partial dislocations, stronger barriers and greater work hardening.

Table 1. Summary of Re Slip Systems.[9, 36, 37, 38, 39]

Type	Glide	Glide	Glide
Slip Direction (most common)	$<11\bar{2}0>$	$<11\bar{2}0>$	$<11\bar{2}0>$
Slip Plane	(0001) Dominant	$(10\bar{1}0)$ Dominant	$(10\bar{1}1)$

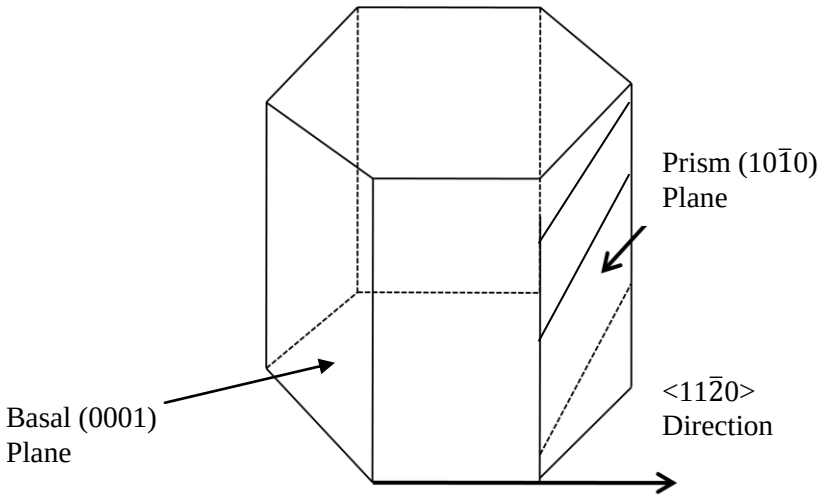

Figure 1. The sketch above shows the dominant Re slip systems.[9]

Dislocation Systems in Rhenium Single Crystals

Subsequent investigators attempted to learn about Re deformation through study of single crystals. Geach, et al.[36], in their work on single crystals confirmed those slip systems Churchman found. However they thought the higher lattice elastic constants of Re were the main reason single crystals of Re are strengthened by plastic deformation rather than intersecting prismatic dislocations. This can be easily understood from the relationship described by Dieter[33] between shear stress, shear modulus of elasticity and dislocation density, $\tau = \tau_0 + \alpha G b \rho^{1/2}$. In this relationship τ is the resolved shear stress required for further plastic deformation, τ_0 is the shear stress required to move a dislocation in the absence of other dislocations, α is a constant (typically 0.3 to 0.6), G is the shear modulus, b the burgers vector and ρ the dislocation density. Furthermore they agreed that additional strengthening of polycrystalline Re results from interaction with neighboring grains. This supports simultaneous dislocation motion on multiple slip systems. Slip in both single and polycrystalline occurs on (0001) and $\{10\bar{1}0\}$ planes and occasionally $\{10\bar{1}1\}$ planes. Finally they confirmed Churchman's contention that crystals, grains, of different orientations work harden at very different rates thus in

polycrystalline materials this differential would be expected to contribute to cracking at grain boundaries.

Stacking Fault Energy

Material with wide stacking faults and consequent low stacking fault energy (SFE) can strain harden easier than those with high stacking fault energy and twin more easily.[33] Since Re exhibits a high strain hardening rate and twins easily, exploration of its SFE is in order.

Churchman's[9] speculated that Re would have low SFE since it has such a high work hardening rate. In contrast Kopetskiy et al.[37] reported that the literature indicates stacking fault energy (SFE) determines whether basal or prismatic slip is dominant. They reported from the literature SFE of 180 erg/cm^2. However using the theory of thermally activated cross slip they found the SFE to be 430 erg/cm^2.

Both of these SFE values are high compared to sample stacking fault energies reported by Dieter.[33] For example he stated 304 stainless steel had 20 erg/cm^2 and aluminum has 200 erg/cm^2. Thus there appears to be more work that could be done to clarify Re SFE. If Re has a high stacking fault energy then Churchman's[9] speculation about low SFE is incorrect. Since the work hardening is high, one would expect greater separation of partial dislocations resulting in stronger barriers.

Twinning

In addition to the dislocation slip systems, a number of authors found twinning to be important in Re deformation.[9, 29, 36-41] Churchman[9] found twinning occurred on $\{10\bar{1}2\}$, $\{11\bar{2}2\}$ and $\{11\bar{2}1\}$ with the last predominating. He also found that the twin intersection points of some of the twins restricted twin growth. From this he concluded

the stacking fault energy in Re was low and that could lead to greater separation of partial dislocations. As a result of this situation, stronger barriers to dislocation motion could result and consequently greater work hardening. Jeffrey and Smith[40] when studying Re single crystals, found that a lower local stress is required for twin nucleation on the $\{11\bar{2}1\}$ plane in polycrystalline Re and are aided by the local stresses resulting from the complex Re slip deformation. Lagerlof et al.[2, 41] contended that deformation twinning is likely affected by the high ductility of Re and its high work hardening rate. They also suggested a twin could form by dissociating a pinned screw dislocation into a partial comprised of a twinning partial that creates a micro-twin that moves on the twin plane and a stationary partial. They contend expansion of micro-twins in combination with double cross-slip of the pinned screw segment could enable lateral twin growth and twin thickening.

Another Re study of single crystals conducted by Kopetskiy et al.[37] correlated mechanical properties with microstructure including dislocations. They found twinning deformation was an important mechanism in the plastic deformation of Re at all temperatures but especially at low temperature. They also found it occurred on $\{10\bar{1}2\}$ $<10\bar{1}\bar{1}>$, $\{11\bar{2}2\}$ $<11\bar{2}\bar{3}>$, $\{11\bar{2}1\}$ $<\bar{1}\bar{1}26>$ with the last two predominating. This will be elaborated on in the next section.

Metallographic analysis by Kopetskiy et al.[37] showed the dominant twinning plane at 4.2 K and 77 K is $(11\bar{2}1)$. If temperature decreases, deformation transitions from second to third stage and critical resolved shear stress increases. This reinforces the notion that shear stress is dependent on temperature. It also increases as the amount of contamination increases as from oxygen and tungsten. It is more pronounced as the temperature decreases.

Table 2. Summary of Re Twinning Systems.[1, 2, 3]

Type	Twin	Twin	Twin
Twin Direction (most common)	$<\bar{1}\bar{1}26>$	$<11\bar{2}\bar{3}>$	$<10\bar{1}\bar{1}>$
Slip Plane	$(11\bar{2}1)$ Dominant	$(11\bar{2}2)$	$(10\bar{1}2)$

Work Hardening (Stress vs. Deformation)

As noted above, Re is ductile but work hardens to a high hardness and significantly increased strength. This results from the internal changes accompanying deformation. Thus discussion of these changes is needed for full understanding of the impact of work hardening operations such as rolling.

Kopetskiy et al.[37] studied single crystals at 4.2 K under a shear strain of 0.5 percent. The stress strain curve exhibits a steep slope approximating a straight line indicative of second stage (conjugate) strengthening. Interestingly Kopetskiy et al. state this is typical of metals with a high SFE and FCC lattice, for example aluminum. Ductility remains high approximately 50 percent. The strain increased dramatically as the orientation departed from the [0001] orientation to a $[10\bar{1}0]$ orientation. Ductility over 50 percent was found at 293 K and 1273 K as the crystal orientation shifted to $[10\bar{1}0]$ but exhibited only 25 percent and 15 percent at 293 K and 1273 K respectively when the orientation was [0001]. Likewise when the crystal orientation was shifted toward the $[11\bar{2}0]$, Kopetskiy et al.[3] reported deformation increased at all temperatures, 45 percent at 4.2 K, 90 percent at 77 K, 280 percent at 293 K and 1273 K.

When loaded in the orientation $[11\bar{2}3]$ but with only limited deformation, Kopetskiy et al.[37] observed that the stress-strain @ 293 K and 523 K tended to divide into three stages: first stage – single slip; second stage – conjugated slip; and third stage – cross slip from basal to prism plane. The initial slip occurs on the basal plane.

Interestingly not all stages appear in all circumstances. Kopetskiy et al.[37] felt this behavior simulated FCC systems.

Geach et al.[36] found the average critical resolved shear stress (CRSS) for Re single crystals, τ_0, for the (0001) to be 14.5 MPa and 21.4 MPa for the $(10\bar{1}0)$ slip plane. Comparing this to other alloys they showed that Rhenium CRSS was low for a material with such a high modulus.

Savitskii et al.[38] found the average critical resolved shear stress for polycrystalline materials (τ_0) to be 1.48 Kg/mm (14.5 MPa)) for pure Rhenium for slip along the basal plane and 2.19 kg/mm (21.4 MPa) for slip along (10-10). Kopetskiy et al.[37] found τ_0 to be 1.8 kg/mm (17.9 MPa) at 293 K and 1.2 kg/mm (11.7 MPa) at 1273 K for pure Rhenium. However for higher contents of oxygen and tungsten, τ_0 was increased to 2.3 kg/mm (22.8 MPa) at 293 K and 3.2 kg/mm (31.0 MPa) at 1273 K. These results may indicate that at higher temperature, diffusion of contaminants is greater and as a result they may be able to interfere with dislocation motion more readily.

Strength, hardness and work hardening vary with orientation. Kopetskiy et al.[37] found significant work hardening in [0001] orientation, if the basal axis is parallel to the tensile axis. No stage of easy slip was noted. Microhardness varies with orientation as reported by Carlen and Bryskin[27] and Papirov and Kapchern.[42]

For $[10\bar{1}5]$ Kopetskiy et al.[37] found work hardening of the second stage is much less than for purely basal slip. The softening associated with twinning at 1273 K makes Re highly ductile.

They also reported that Savitskiy[38] found oxygen that intruded into the Re lattice, lowered its plasticity by jamming the normal slip systems but new slip systems could be activated at higher stresses.

Table 3. Hexagonal Metal Average Critical Resolved Shear Stress Metals.[2]

Metal	τ_0 (MPa), (0001)	τ_0 (MPa), $(10\bar{1}0)$
Be	13.8	65.5
Ti	62-103	13.8-89.6
Zr	>31.0	9
Re	14.5	21.4

As mentioned earlier Re has a high modulus. When that modulus is compared to other hcp metals with elevated temperature melting points, the comparison shows the CRSS is low for a material with a high modulus of elasticity. See Table 3.

A review of critical resolved shear stress shows it is related to the Peierls – Nabarro Stress relationship.[35] It is the stress to move one dislocation and is as follows:

$$\tau_{PN} = \alpha(Gb/2c)e^{-(\pi a/c)} \sin(2\pi x/c)$$

Where: c is the spacing of atoms in the x direction, a is the lattice parameter, α is a parameter depending on the barrier nature and G is the shear modulus. The shear and tensile modulus are related as follows*: $G=E/(2(1+\upsilon))$*

Rolling Effects

A PM ingot can present problems to manufacturing operations. For example, when shapes contain unintened porosity, the microporosity may consolidate to form larger pores of unacceptable size[30] when welded. However sufficient reduction through rolling will reduce the porosity significantly if not eliminate it entirely.[29, 39] When rolling, the typical practice is to deform the plate approximately 10 percent or even slightly less,

then annealed. This prevents cracks and reduces the loads needed to deform the material.[13] Carlen and Bryskin[27] actually found they could reduce polycrystalline plate up to 15 percent without noticeable cracking. From an operations stand point, a more conservative 10 percent reduces cost by reducing the load of rolling and reducing the likelihood of lost plate due to cracking. Ten percent is less reduction between annealing than most metals.[27] This iterative process continues until the ultimate amount of reduction is achieved. Finally Carlen and Bryskin[27] found microcracks initiated at grain boundary triple points during rolling which they suggested were the weakest areas.

Larikov et al.[39] in their study of rolling effects on single crystals supported Churchman's[9] contention that the high rate of work hardening in Re results from intersection of prismatic glide systems by $\{\bar{1}0\bar{1}0\}$ planes. They found that after deformation of as little as 8 percent, the single crystal transformed into polycrystalline form as evidenced by transformation of discrete x-ray Laue reflections into diffuse rings. They also reported that Re deforms by twinning in the $\{11\bar{2}2\}$, $\{10\bar{1}2\}$ and $\{11\bar{2}1\}$ planes as did Kopetskiy et al.[37] In the region surrounding the twin they found high local stresses. As a probable result of the high local stresses, the slip lines and new twins are nucleated on the periphery of the twins.

Using density measurements Larikov et al.[39] studied the formation of microcracks and found the density constant up to approximately 20 percent deformation. Between 20 percent and approximately 23 percent, deformation is somewhat gradual but noticeable. Above 23 percent the density drops dramatically till approximately 25 percent where the slope becomes almost flat at 28 percent deformation. At deformations greater than 28 percent, cracks begin to form on the surface and propagate into the crystal. Below

28 percent microcracks formed most likely due to the high work hardening rate and intensive twinning.

With sufficient deformation Larikov et al.[39] also found the Re single crystal transforms to polycrystalline morphology. The growth kinetics of the recrystalizing grains can be described by a parameter $G_{gr}=c\varepsilon^{n}$ where c and n are constants and ε is strain. Below 30 percent strain n=2.2 and above 30 percent. Larikov et al.[39] contend that a high driving force results from the stored energy from deformation. Another way to view the parameter G is in terms of diffusion and chemical potential. It can be expressed as $G=(D_{qb}/kT)(\Delta M/\Delta x)$ Where $(\Delta M/\Delta x)$ is the gradient of the chemical potential, the driving force of the grain growth process. D_{qb} is the coefficient of the boundary self-diffusion and (D_{qb}/kT) is the mobility of the growing grain boundary. Another perspective about this is that the high degree of hardening for deformations > 28 percent accelerates recrystalization due to the stored energy from deformation.

Recrystalization nucleation accelerates once surface cracks are produced since the local deformation is highest near the microcrack. In addition twin lamellae often are found to be the site of grain nuclei. The growth of recrystallized grains can be restricted by microcracks with the restriction increasing as the spacing of microcracks decreases. Larikov et al.[39] note that the grains boundaries are often stepped.

Studies indicated that internal microcracks can be eliminated by thermal treatment.[39] This phenomenon was noticed when the density increased with annealing. However the branched microcracks reaching the surface were not eliminated. They suggest that the internal microcracks were eliminated by diffusion along the surface of

the internal microcracks. Most likely the surface cracks were not eliminated due to contamination from the furnace environment.

Metallographic Characteristics

Kopetskiy et al.[9] correlated mechanical properties with microstructure including dislocations. They performed tensile tests with effective load applied in the [11$\bar{2}$3], [10$\bar{1}$5] and [0001] directions. Twin deformation occurred on {10$\bar{1}$2} <10$\bar{1}\bar{1}$_>, {11$\bar{2}$2} <11$\bar{2}\bar{3}$> {11$\bar{2}$1} <$\bar{1}\bar{1}$26> with predominance of the latter.

As they studied the metallographic [11$\bar{2}$3] orientation, Kopetskiy et al.[9] found the dislocation structure at 4.2 K and 77 K to exhibit thin lamellae whose density increased as the strain increased. Between lamellae they found isolated dislocations, dislocation loops, dipoles and elongated clusters. Dislocations stretched in a certain direction usually [01$\bar{1}$0]. Clusters of dislocations are stress concentrations which may give rise to twin lamellae. Twin interlayers and dislocation bands were observed at all stages of the stress strain curve from 77 to 1273 K

Twinning was the predominate factor in plastic deformation at 4 and 77 K more than at other temperatures.[37] The twins are replaced by large numbers of irregular dislocation clusters and networks at 773 K and 1273 K. They did, however, report some dissociation. Density of twin lamellae and dislocation bands grew gradually with plastic deformation at RT (293 K). Twin lamellae and dislocation bands usually occur in one [10$\bar{1}$0] direction. Between lamellae and dislocation bands are large groups of dipoles and complete prismatic dislocation loop, apparently formed during deformation without diffusion since deformation temperature was 0.8 Tmp.

The density of twin lamellae and dislocation dipoles become less than at the same stages of deformation at lower temperature and a large number of irregular dislocation clusters and networks appear at 773 K and particularly 1273 K. At 1273 K a large number of disassociated dislocations were observed and, irrespective of the amount of deformation, were still there after annealing at 1273 K. Kopetskiy et al.[37] speculated that this could be due to temperature or contamination such as from oxygen, tungsten, etc.

Rhenium Physical and Mechanical Properties

As noted in the section discussing processes, different component manufacturing processes produce different properties.[1, 5, 6,7, 26, 31-32, 43-56] All metals, as well as pure rhenium mechanical properties, are related to the microstructure produced by those properties such as grain size, grain morphology, grain orientation, amount of cold work, etc.[33,34,35] However a generally accepted set of baseline properties will be valuable in exploration of the difference in rhenium properties as influenced by process.

Table 4. Summary of Typical Properties.[1, 5, 6, 7]

Property	Value
Melting point	3180 °C
Density	21.0 g/cm^3
Modulus	460 GPa
Strength	Moderate to high
At RT	YS (.2 percent) 207 MPa
	UTS 759 MPa
	Ave. wrought Strain to failure 13 percent
	Wire UTS> 2 GPa
At 2204°C	UTS 48 MPa
Wear Resistance	High
Oxidation Resistance	Poor-Pure metal oxidizes at low temperature and produces a volatile oxide, Re_2O_7, at approximately 360 °C
Aqueous Corrosion Resistance	Rhenium is very resistant to seawater, many acids and hot gases in neutral or reducing environments
Work hardening rate	High

Before comparing property differences resulting from different rhenium manufacturing processes, it would also be instructive to compare some Re properties to other elements commonly used for structural purposes, particularly those elements with an hcp structure and relatively high melting points. Note the drastic difference in modulus and melting point of Re compared to the other hcp elements.

Table 5. Comparison of Re Properties to Other hcp Materials.[1, 5, 6]

Property	Re	Zr	Ti	Be
Young's Modulus GPa	460	99.3	110.3	296.5
Shear Modulus GPa	177.9	34.5	45.5	137.9
Density g/cm^3	21.0	6.5	4.5	1.8
Poisson's Ratio	0.296	0.360	0.340	0.07
Melting Temperature	3180 °C	1825 °C	1668 °C	1278 °C

Comparison of Mechanical Properties and Description of Fracture Features from Various Processes

Tensile Strength

Biaglow[31] of the NASA Research Center (LeRC) studied the mechanical properties of chemical vapor deposition (CVD) and powder metallurgy (PM) in several different forms. The powder metallurgy samples were in the form of rolled sheet, pressed

and sintered bars, and hot isostatic pressure (HIP) product. Tensile test temperatures were RT, 1088 K and 1644 K. At RT the powder metallurgy tensile values ranged from 663 MPA to 943 MPa, with a range of strain to failure of 11.2 percent to 27.5 percent. See Table 6. At elevated temperature the strength was good but the elongation fell dramatically. In fact, at 1644 K the strain to failure falls below 5 percent and, in several cases, fell below 1 percent. See Table 12 for more details. Chazen[32] also compared Re powder metallurgy samples to Re chemical vapor deposition samples. Tests were conducted at room temperature (RT), 1088 K and 1644. Similar results were obtained. At RT the CVD UTS ranged from 661 MPa to 674 MPa as compared to the powdered metallurgy samples which exhibited ultimate tensile strengths from 676 MPa to 841 MPa. The strain to failure also indicated good ductility with the CVD samples ranging from 9 percent to 27.5 percent elongation and the PM samples had elongation of 9.8 to 16.2 percent. The CVD PM samples tested at 1088 K exhibited UTS of 429 MPa to 482 MPa. At this temperature, the strain to failure ranged from 9.3 percent to 25 percent, similar to the RT strain to failure values. At 1644 K the PM strengths were noticeably lower than the CVD sample. They had strengths at approximately 208 MPa compared to the CVD strengths that ranged from 145 MPa to 367 MPa. Temperature strongly affected the elongation and reduced it to below 5 percent for all samples but the CVD elongation was below 2 percent with a value as low as 0.3 percent.

Robinson et al.[43] studied the mechanical properties of cold rolled plate, that was diffusion bonded together and hot isostatically pressed plate. The cold rolled and bonded specimens are representative of the manner of fabrication of Re components. Tabs were welded to the bonded stack and tensile specimens were created so that the axis of load was perpendicular to the bond lines. Testing took place at 1644 K to explore ductility

since, as noted in previous tests, the ductility can be low at elevated temperature. The cold rolled and bonded specimen tensile strengths ranged from 179 MPa to 248 MPa with elongations ranging from 3 to 11 percent. The HIPed specimens had strengths ranging from 324 MPa to 338 MPa with elongations ranging from 12 to 19.5 percent.

Unlike some other refractory materials, Re has no brittle-to-ductile transition temperature. Kopetskiy et al.[37] showed that Re specimens had nearly 50 percent elongation at 4.2 K.

Biaglow[31] found the rolled sheet samples failed with noticeable macro-deformation and intergranular micro-features below 1644 K. At that temperature the micro-fracture features were predominately intergranular but mixed with some dimples features. HIPed samples showed no macro-deformation at any temperature. The CVD samples exhibited noticeable deformation but jagged fracture features that appeared to jump from different layers. The surface also had elongated surface features indicative of the columnar structure of CVD Re.

At room temperature Chazen[32] found the CVD sample fractures were predominately intergranular with some dimple rupture. For PM components the predominate fracture mode is intergranular from room temperature up to approximately 815 °C. Above this temperature, the fracture mode appears to change to a dimple rupture mode.[32]

Robinson et al.[43] studied cold rolled (CR) and HIPed tensile properties at 1371 °C. They found the CR samples' fracture features had an intergranular outer skin and mixed mode intergranular and transgranular fracture features at the specimen interior. The PM sintered and HIPed exhibited dimple rupture fracture features throughout when

tested at 1371 °C. However, the fracture samples also exhibited cracking below the fracture surface after deformation of the order of 12-to 19.5 percent. They found most of the cracking along the grain boundaries.

Arcella et al.[18] performed limited testing of LAM Re at RT and found the ultimate tensile strength and yield strength were both lower than Re from other manufacturing processes. However, the elongation at room temperature was much higher than the comparable elongation for the other processes. The testing did indicate some directionality. See Table 6. The Arcella study did not include any elevated temperature testing nor did they offer any explanation of the high elongation found, nor insight into deformation or fracture mechanisms. Additional work will be required to fill this gap.

Table 6. Room Temperature Properties of Re.[31]

Type	UTS (MPa)	YS 0.2 percent (MPa)	Percent Strain to Failure
HIPed	910.8	238.5	17.2
HIPed	915.8	232.4	18.5
Pressed and Sintered	677.8	227.5	9.8
Pressed and Sintered	757.8	206.8	13.2
CVD	688.1	308.8	21.9
CVD	697.8	284.5	19.4
Rolled Sheet	921.9	568.1	16.4
Rolled Sheet	943.2	500.9	17.2
RAI PM CR	971.4	483.3	36.2
RAI LAM Re, Long.	595.7	326.1	63.8
RAI LAM Re Trans.	326.8	188.2	27.7

Table 7. Elevated Temperature, 1371°C, Properties of Re.[31]

Type	UTS (MPa)	YS 0.2 percent (MPa)	Percent Strain to Failure
HIPed	215.8	179.9	2.28
HIPed	251.8	191.0	4.49
Pressed and Sintered	208.2	151.7	4.2
Pressed and Sintered	202.0	144.8	4.3
CVD	455.8	344.7	3.11
CVD	289.6	266.8	0.411
Rolled Sheet	419.2	366.8	0.80
Rolled Sheet	443.3	370.1	1.38

Room Temperature Fatigue Strength

Limited studies have been found in the literature about Rhenium fatigue properties. Biaglow [38] studied low cycle fatigue of Re produced from both CVD and powder metallurgy processes. His results are noted in Table 8.

Table 8. Biaglow RT Fatigue Tests.

Sample Type – No. of Samples	Stress (MPa) Tension/Compression	Cycles Completed When Test Stopped
CVD -2	151.7/151.7	100
PM – 2	206.9/206.9	100

Little details about experimental procedure were available including a lack of information about fatigue sample orientation. The samples had comparatively low density

of 95 to 96 percent density. Chazen also conducted fatigue test with Re produced from both CVD and powder metallurgy processes and his results are listed in Table 9.

Table 9. Chazen RT Fatigue Tests.

Sample Type – No. of Samples	Stress (MPa) Tension/Compression	Cycles Completed When Test Stopped
CVD – 2	152	100
PM – 1	207	100
PM – 1	190	100

Both studies arbitrarily stopped the tests at 100 cycles.

Indentation Testing

Indentation testing for Re and especially LAM Re is limited. Pairov et al.[42] found the hardness on crystals with known orientation. The microhardness varied from 160 kg/mm^2 (1.6 GPa) to 430 kg/mm^2 (4.2 GPa). Arcella et al.[17] found the hardness varied form 310 kg/mm^2 to 580 kg/mm^2. No indication of orientation was offered. No nanoindentation testing of Re or LAM Re was found in the literature. Correlation of indentation testing with Young's modulus was also absent from the literature.

3. RESEARCH OBJECTIVES AND APPROACH

The literature review indicated that many of the rhenium products from different fabrication processes have been investigated. The work characterizing Laser Additive Manufactured (LAM) rhenium or any additive manufactured rhenium is limited. Grain size and morphology as well as temperature affects the fracture mode of other types of Re, but no such information has been found for LAM Re. Very limited information describing the effect of loading concentrated in a small area has been found. Such information is potentially important for evaluating thin layers of Re. The work proposed will fill these gaps and is described below.

Determine the affect of LAM Re processing on microstructure including crystallographic orientation. Other Re manufacturing processes affect microstructure and, as a result, deformation. Determination of the affect of LAM's unique processing on microstructure must be completed before the microstructure effect on deformation and mechanical properties can be undertaken in other efforts. Grain size and shape influence deformation but so will the crystallographic orientation. Re has limited deformation systems and orientation can affect not only deformation but elastic modulus as well. Optical microscopy and OIM will be employed to gather this data.

In spite of the extensive reporting about Re bulk microstructure in the literature, very little study of LAM Re or any AM Re has been found. No correlation with crystal orientation has been located. In fact no orientation image mapping (EBSD) of any type of Re has been seen in the open literature to date.

Determine the impact of the Re deformation systems, slip and twinning, on localized deformation using nanoindentation. This study will measure hardness and

Young's modulus and the crystal orientation at the point of indentation. Comparing this data to information in the literature will lead to a better understanding of Re's deformation mechanisms when a load is applied to a small localized area.

The literature presents limited information about Re deformation under local loading as opposed to bulk deformation and none has been found about nanoindentation. Some microhardness testing has been found. The experiments will to determine if nanoindentation testing of Re reflects the mechanical values found for bulk Re or if any anomalies occur when nanoindentation tested, since it has such a high work hardening rate and twins easily. This information should assist understanding the response of Re to concentrated loading.

Determine the bulk mechanical properties of LAM Re. The effect of temperature, including ultra-high temperature tensile testing of bulk samples, on deformation mechanisms and fracture modes will be studied. Define ultra-high temperature as greater than or equal to 1648 °C and above, then no testing of conventional Re or pure LAM Re at these temperatures has been found in the open literature. Some fatigue samples will be tested at room temperature to determine LAM Re's response. Limited information about Re fatigue is available in the literature. Fractography of all specimens will be undertaken to determine fracture features to shed light on LAM Re deformation and fracture mechanisms.

Characterize Microstructure

Grain Size and Morphology

Optical microscopy will be used to study the grain size and morphology of LAM Re. First a polishing procedure must be developed. Re deforms easily and work hardens

readily. Deformed surfaces can be created with an aggressive polishing procedure and artifacts introduced to the surface. Introduction of unintended artifacts is also a concern for OIM and is discussed below. Once the procedure is available, sections from tensile bars will be removed, mounted and polished. The microstructure will be documented for three orthogonal views.

Crystal Orientation

The same mounts will be used for OIM study after optical examination is complete. OIM is very sensitive to surface disturbance. Deformation unintentionally induced into the surface from polishing can preclude generation of useable OIM signals. OIM will be used to assess crystal orientation by determining plane indices for the polished surface. Then these indices will be used to calculate Young's modulus.

Determine Nanoindentation Properties

Mechanical Property Extraction from Nanoindentation Measurements

Nanoindentation measurements will be made on the same samples used for microstructure characterization. The research effort will determine Young's modulus, hardness and compressive strength. One of the potential applications of additive manufacturing is deposition of thin graded structures. Understanding the deformation properties of thin layers of Re will be important for effective future use and will fill gaps of information in the literature.

Bulk Mechanical Properties of Re

Testing at Ultra-High Temperatures and Fractography

Facilities to test at ultra-high temperatures are limited. Experimentation will perform initial testing at Southern Research Institute. While that is in progress,

preparation for testing at a local facility will begin. Custom tooling for the load train has to be designed and manufactured.

Testing will be performed at 1371 °C and 1925 °C. The strength parallel to the build direction will be tested as well as that transverse to the build direction to determine if any property orientation exists. Fracture features for tensile specimens will be determined and compared to that found in the literature. Analysis of this data will give insight into deformation and fracture mechanisms.

Fatigue Testing and Fractography

Fatigue testing at RT will be performed both parallel to build direction and transverse to build direction. Fracture surfaces will be examined to determine fracture features and understand fracture mechanism.

4. CHARACTERIZATION

Introduction

Laser additive manufacturing is an AM system which supplies high energy in the form of laser light at the intersection of the flowing feed stock and the work piece.[17, 18] The laser has very high power capable of supplying a maximum of 18 kilowatts. High power provided by LAM is well suited to fusing the high melting point Re feedstock. The laser and feedstock enter separate columns at the top, progress down the columns and exit at the bottom at the work piece. The system not only has high power but also is physically large. See Figure 2 and Figure 3 where the man stands on the edge of the system. Deposition atmosphere is an inert gas, typically argon.

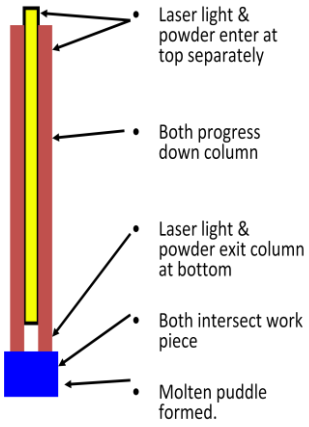

Figure 2. Major components of a Laser Additive manufactured system.[17, 18]

Figure 3 Photograph that shows AeroMet Laser Additive Manufacturing system.[18]

Chemical Analysis

Chemical analysis was undertaken to verify the composition of the samples and to insure there is no tungsten (W) or other contamination present. The latter is masked in some techniques. At the time of deposition a significant amount of Re W was being produced at the facility.

Materials and Experimental Procedure

One sample with tungsten was tested to ensure that the output without tungsten was accurate. Several techniques were employed since not all are equally sensitive to W. For example, energy dispersive x-ray (EDX) analysis does not sense W in Re in the low percent range. On the other hand X-ray Photoelectron Spectroscopy (XPS), also known as ESCA shows W in the presence of Re as does wavelength dispersive x-ray spectroscopy (WDS). To complete quantification of impurity levels, multiple techniques were used. Quantitative chemical analysis using inductively coupled mass spectroscopy (ICP/MS) for most elements was used. Leco combustion for carbon, hydrogen, nitrogen and oxygen techniques and DC arc for potassium, sodium and silicon was employed.

Results and Discussions

XPS indicated the presence of W in the W containing sample; hence its analysis of pure Re was deemed accurate. See Figure 4.

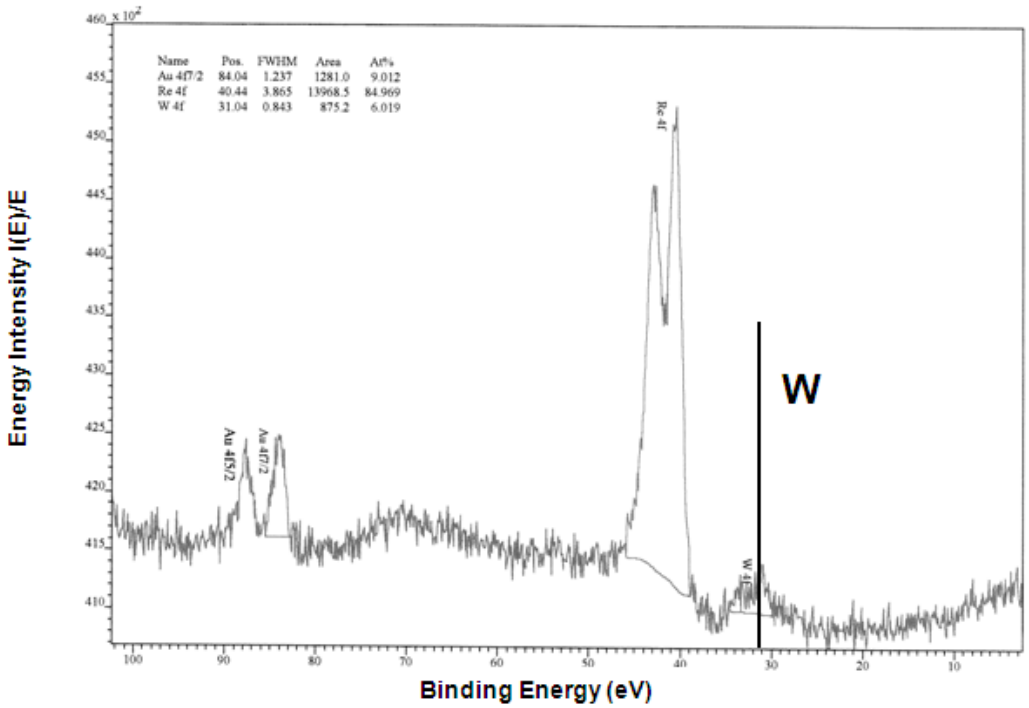

Figure 4. XPS Spectrograph Graph showing the presence of tungsten.

WDS confirmed the XPS results since it displays W. See Figure 5 to see the combined EDS output with WDS output. Note the EDS Re signal masks the W signal.

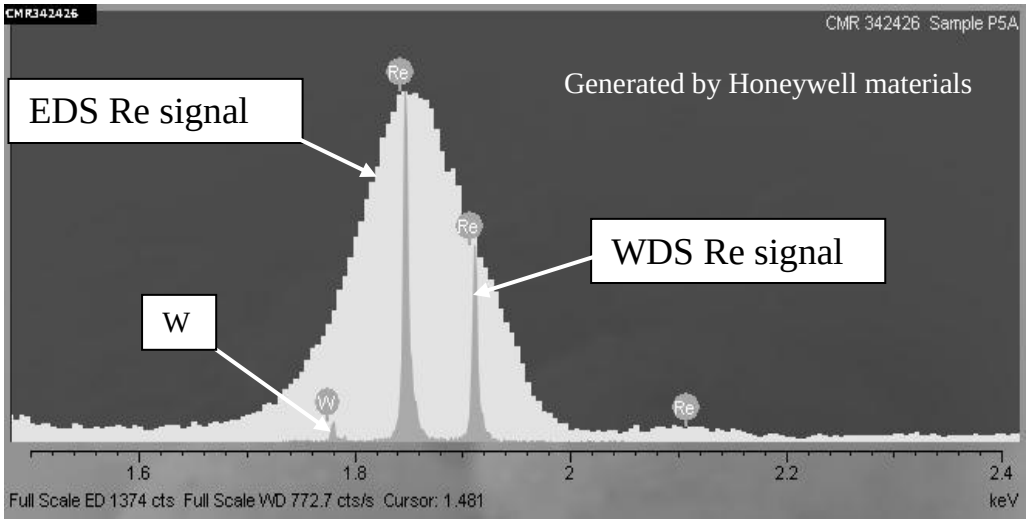

Figure 5. WDS and EDS clearly reveal the presence of W in the WDS graph but not the EDS graph. The large white peak is the Re EDS spectrum and the gray peaks are the WDS output.

Finally to ensure complete accuracy, quantitative chemical analysis was undertaken at a commercial laboratory specializing in that work, NSL Analytical. Forty elements were analyzed besides Re. All elements were found in only low parts per million (ppm) with the highest being W at 310 ppm and the balance was Re in the pure Re sample. The W containing sample had 36600 ppm.

Microstructural Characterization

LAM Re plates are deposited in layers along the x-axis about 152 mm, they are built vertically in the z-axis approximately 75 mm and are approximately 9 mm thick in the y direction. See Figure 6. As mentioned in the section discussing processes, a variety of approaches are used to produce Re plate and one of the more common is HIP, roll and anneal. If the anneal takes place above the recrystallization temperature approximately equiaxed grains are produced as in Figure 7.

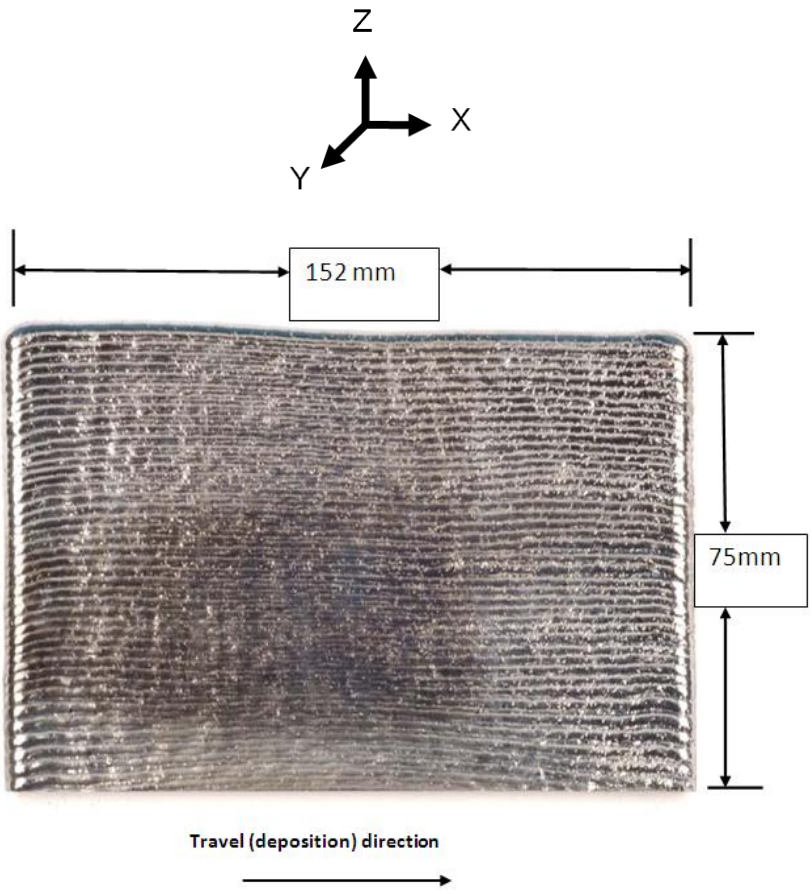

Figure 6. As-deposited LAM Re plate.

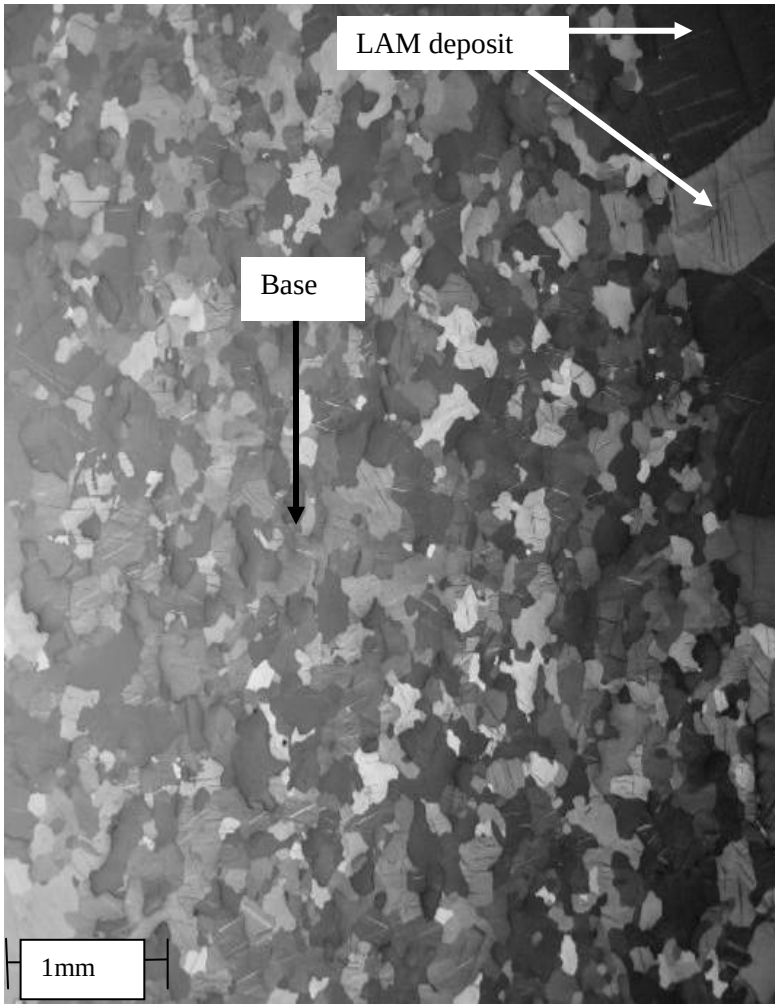

Figure 7. Typical wrought equiaxed grains found in PM or PM HIPed shapes. Used as the starter base for the plate deposited in Figure 4.

The LAM process, on the other hand, deposits the plate through deposition of a series of layers. The plate is continuous and can be used as deposited. Subsequent heat treatment and working are an option.

Materials and Experimental

Metallographic samples were taken from the sides of pure LAM Re tensile specimens at the gauge section for correlation with tensile properties. They were polished and observed through polarized light.

Results and Discussion

LAM deposits Re using high heat input, consequently the grains cool slowly and are quite large; as much as ASTM 00. The grains are equiaxed in the X-Y plane but elongated in the build direction. When viewed perpendicular to the Z or vertical build direction, i.e. in the X-Y plane, the grains appear equiaxed as displayed in Figure 8. However, when the samples are viewed in planes ninety degrees to the X-Z or Y-Z planes, i.e. perpendicular to the travel direction of deposition but with the view plane parallel to the build direction, the grains are elongated as displayed in Figure 9 and in Figure 10. Furthermore, when inspecting the X-Z plane, the grains are not only elongated but form an S pattern as shown in Figure 9. This results from change of deposition direction of one layer relative to the layer below it. Note that the grains are continuous through the deposition direction change. Thus, the knee in grains viewed perpendicular to the X-Z plane mark the plate layers. Another important aspect to note is the grain size. They are quite long passing through multiple deposition layers parallel to the build direction. In addition, the width is sufficiently large that the grains can be seen without aid of magnification. Figure 11 shows a three dimensional view of the microstructure depicted in Figure 8, Figure 9 and Figure 10.

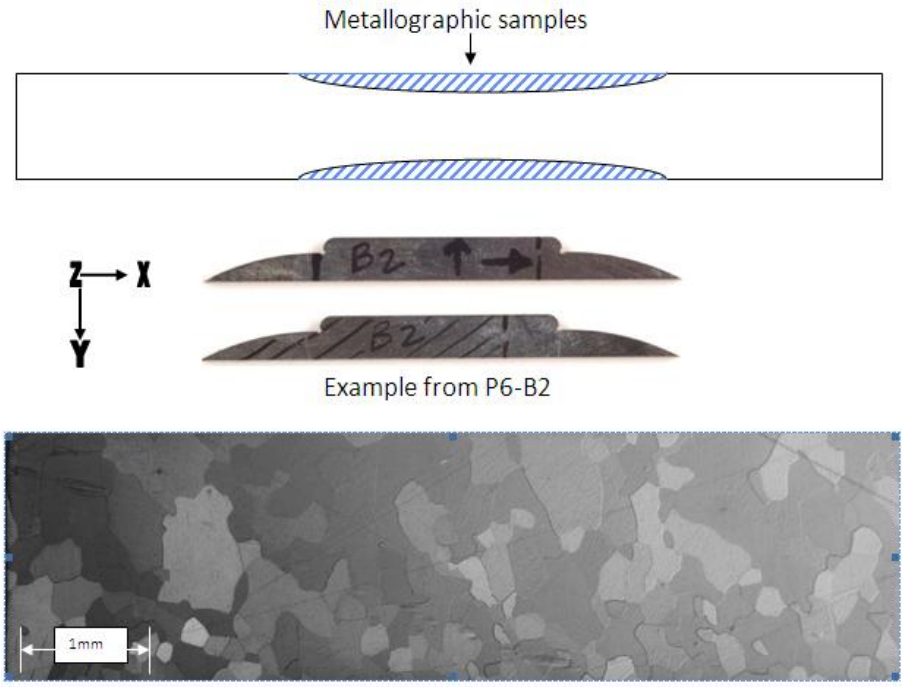

Figure 8. LAM Re microstructure in the Y-X plane showing approximately equiaxed grains.

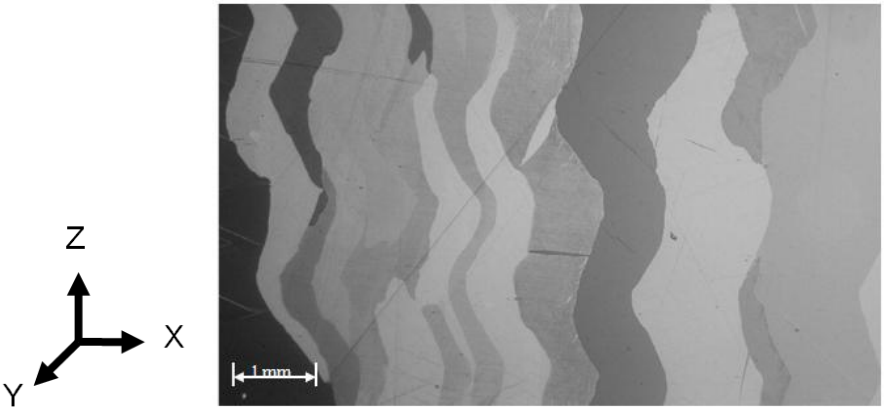

Figure 9. LAM Re microstructure in the X-Z plane, showing a characteristic wavy pattern in the build direction.

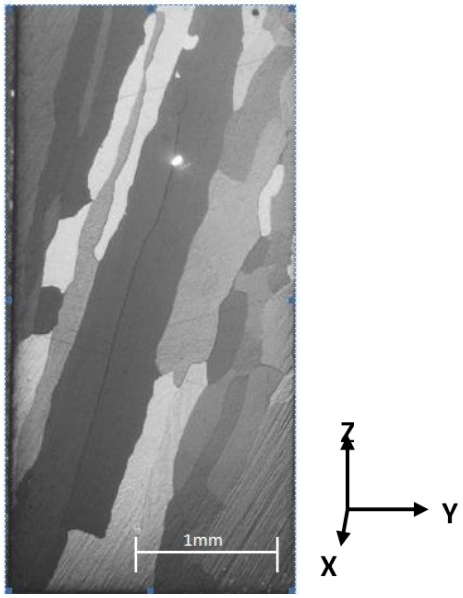

Figure 10. Cross-section of LAM Re microstructure in the x-z plane.

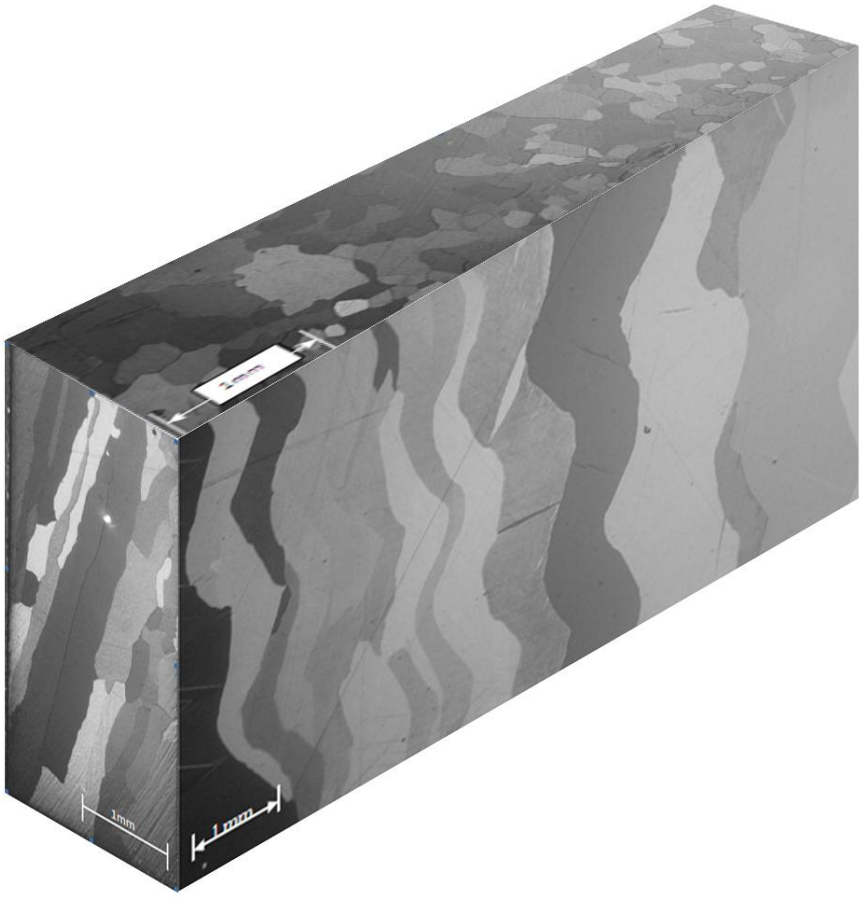

Figure 11. Three dimensional view of pure LAM Re microstructure.

Orientation Image Mapping

Re single crystals are anisotropic. As such its properties are directional in each grain. Since the grains in LAM Re are very large the properties may be more directional than wrought material. Thus it is valuable to determine the relative orientation of the grains.

Materials and Experimental Procedure

Orientation Image Mapping (OIM) collects backscattered electrons to determine crystal orientation.[59] The sample is polished, oriented vertically at seventy degrees to the horizontal but facing a photographic detector. Primary electrons impinge on the sample

surface and some of the electrons are scattered to the detector. These backscattered electrons generate patterns from which crystallographic orientation can be deduced. Figure 12 shows a schematic of the concept of OIM. OIM is also called Electron Backscatter Diffraction (EBSD).

The images shown in this report were produced by a TexSEM Laboratories (TSL) EBSD system mounted on a Fei XL30 scanning electron microscope (SEM).

Re is a soft material and easily deforms, especially during polishing. Special care must be taken to remove all cold work from the surface otherwise no coherent patterns will be generated. The preparation entails extended polishing time during the last stages of polishing to remove the last vestiges of deformed surface layer.

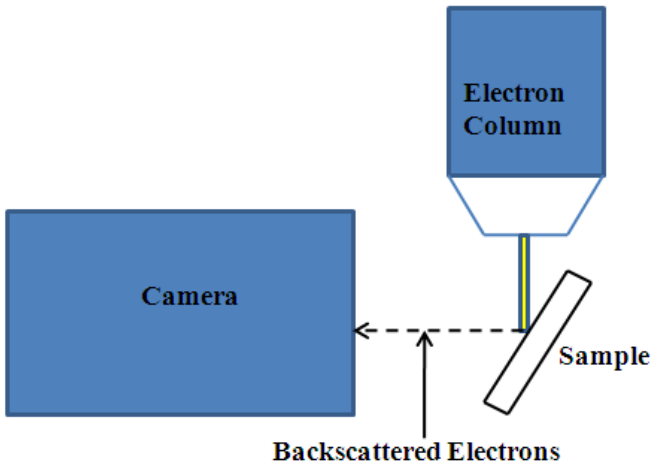

Figure 12. Schematic of the electron back scattered diffraction (EBSD) arrangement.[62]

After the orientation planes are determined they are converted to Miller-Bravais indices from Miller indices. The direction cosines are calculated. The details of calculation are discussed below.

To calculate Young's modulus from OIM data, the following procedure is employed:

Determine indices of planes near the specimen surface using OIM. See Figure 17.

Acquire elastic constants.[60-62]

Calculate direction cosine of plane near specimen surface relative to basal plane (c axis) using Miller-Bravais formula to calculate plane angles in hcp between basal plane and plane of interest.[63]

$$\frac{[hh'+kk'+1/2(hk'+kh')]a^{*2}+ll'c^{*2}}{[(Q_{hkil})(Q_{h'k'l'l'})]^{1/2}}$$

Use Young's modulus formula[64] to calculate E as noted below.

$$(1/E_i) = (1-l_3^2)^2 s_{11}+l_3^4 s_{33} + l_3^2(1-l_3^2)(2s_{13} + s_{44}) \text{ in } GPa^{-1}$$

E depends on crystal direction.

l_3= Direction cosine of the angle between the plane of interest and the basal plan (z axis) of the crystal.

Compare calculated Young's modulus to that measured by nanoindentation.

To verify this approach, the calculation for zinc in Nye and other literature was duplicated.

Results and Discussion

The procedure described above was used to calculate the grain orientation by using the surface crystal indices to deduce Young's modulus. Indices detected using OIM

with calculated moduli related to indentation number are shown in Table 10. The table also includes related information for the major planes. Nanoindentation can then be used to test the calculated value for Young's modulus for that grain and is discussed in the next section.

A sample OIM image is shown in Figure 13 showing a small portion of the grain near indents 10-12. The view magnification was 1500 X. At this magnification small fluctuations in local orientation become noticeable and are highlighted by the wire frame hcp figures where the direction of the "C" axis of each wire frame indicates orientation. The majority of the wire frame images are oriented in the same direction. A schematic of a plane with indices approximating a prism plane is shown in Figure 14 with associated moduli.

Most images were taken at much lower magnification to collect data about overall trends in crystal orientation. Representative OIM images are correlated with microstructure from orthogonal directions and are shown in Figure 15 and Figure 16. The first set of images in Figure 15 shows the equiaxed grain shape first revealed optically in the X-Y plane. One of the trends found in LAM Re was crystal growth through additive layers clearly shown in Figure 16. The knees of the bends in the continuous crystals are the line of adjacent layers. Crystal (grain) tilt in a direction opposite that below the knee indicates a direction of travel opposite that of the layer beneath it.

The OIM pictures shown are representative of crystallographic orientation related to the grain pictured above them but from different samples. OIM confirmed the observation from optical microscopy that as shown Figure 15, the grains are equiaxed in the X-Y plane. In the X-Z plane the representative crystals grow through layers and are

elongated in the Z direction, as shown in Figure 16. No distinctive trend in crystallographic orientation has been observed.

Table 10. OIM Measured Plane Indices vs. Calculated Modulus of Selected Grains.

	OIM Detected Indices					
Indent Number	h	k	i	l	Young's Modulus – E (GPa)	Avg. E (GPa)
1	-15	7	8	18	427.9	428.2
1	0	-8	8	-13	428.7	
1	16	-1	-15	24	428.1	
1	-16	2	14	21	427.9	
5-6	-27	18	9	-5	470.6	472.0
5-6	3	5	-8	1	472.4	
5-6	31	-12	-19	4	472.3	
5-6	9	-4	-5	1	472.7	
10-12	-17	11	6	-4	468.7	470.0
10-12	-6	4	2	-1	471.2	
14	-1	0	1	-6	534.4	534.4
14	-1	0	1	-6	534.4	
56-57	-6	11	-5	18	432.8	432.6
56-57	-9	16	-7	26	432.5	
62-63	-12	3	9	-31	461.8	461.4
62-63	-5	1	4	-13	460.9	
77-78	11	15	-26	-16	447.1	444.8
77-78	3	4	-7	-5	441.7	-
77-78	9	13	-22	-15	443.5	-
77-78	-19	-26	45	-28	446.7	-
Basal Plane	0	0	0	1	587	-
Prism plane	1	0	-1	0	474	-
Pyramidal Plane1-1	1	0	-1	1	435	-
Pyramidal Plane 1-2	1	0	-1	2	435	-
Pyramidal Plane 2-1	1	1	-2	1	454	-
Pyramidal Plane 2-2	1	1	-2	2	431	-

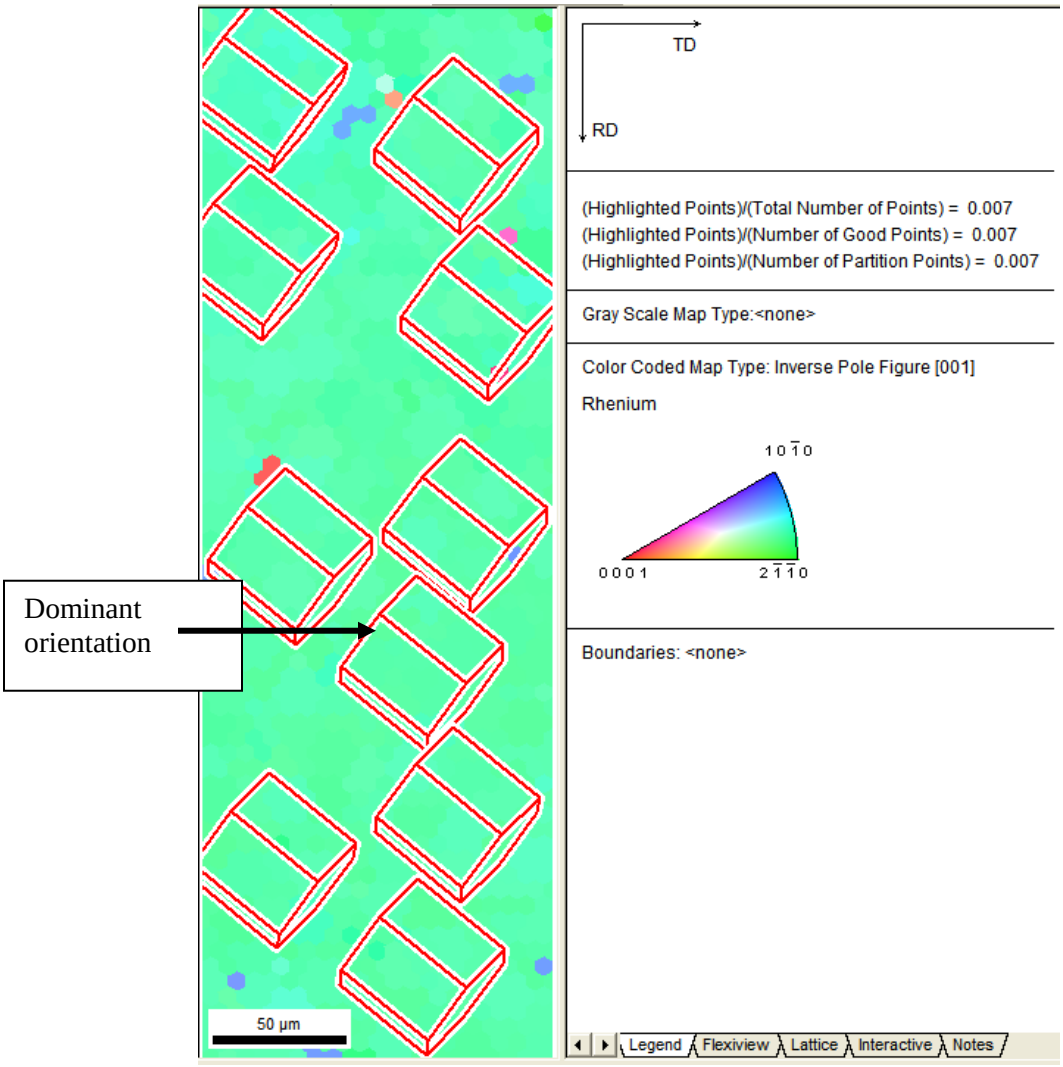

Figure 13. OIM image a small area of a pure Re grain in the X-Z near indents 10-12. See Table 10 for indices and moduli. See Figure 15 for a view of a much larger area.

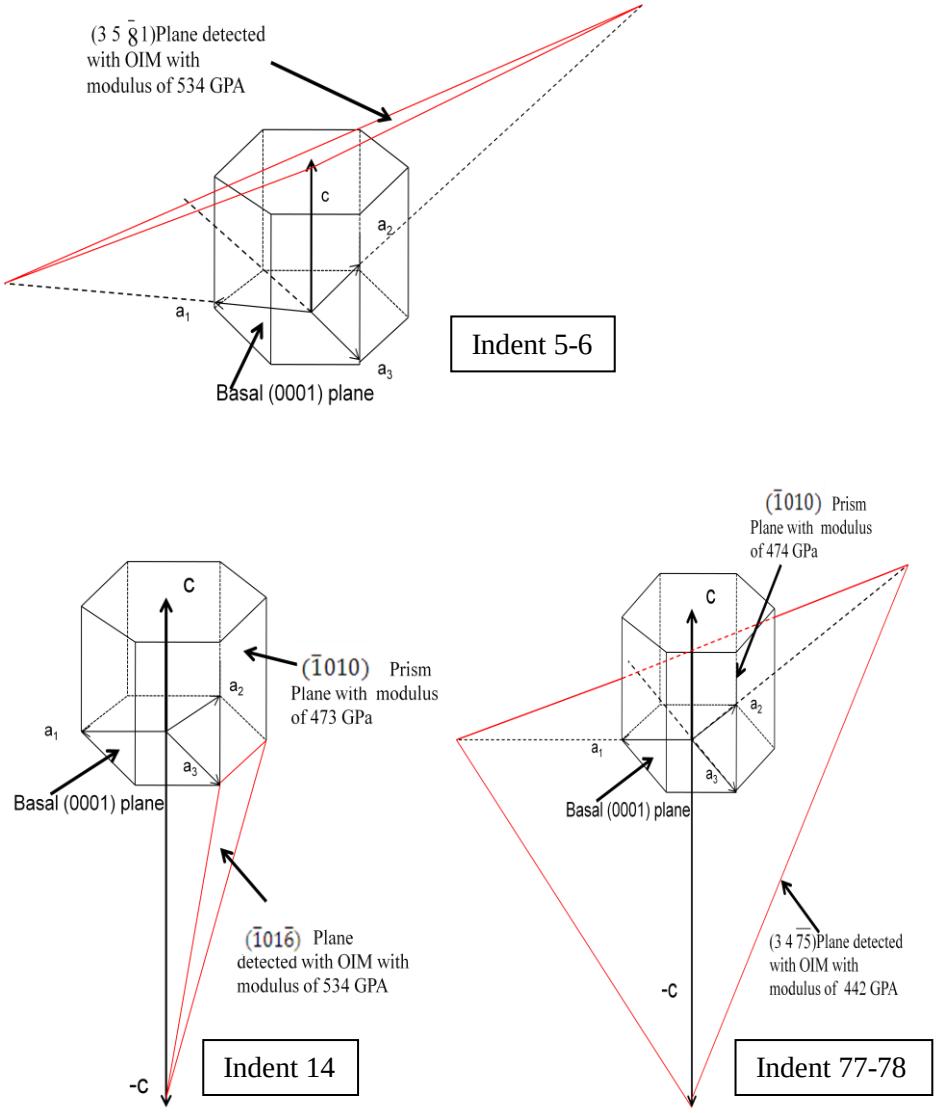

Figure 14. Schematic image showing an OIM detected plane and modulus that approximates a major plane. Moduli for both are shown.

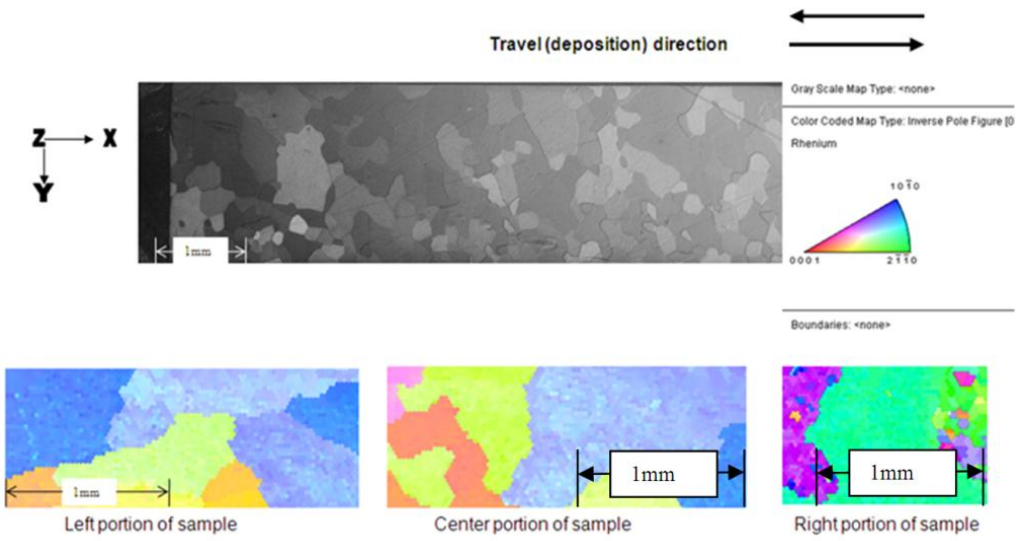

Figure 15. Compare representative equiaxed grain structure of the X-Y planes to representative samples of crystal orientation also for X-Y planes.

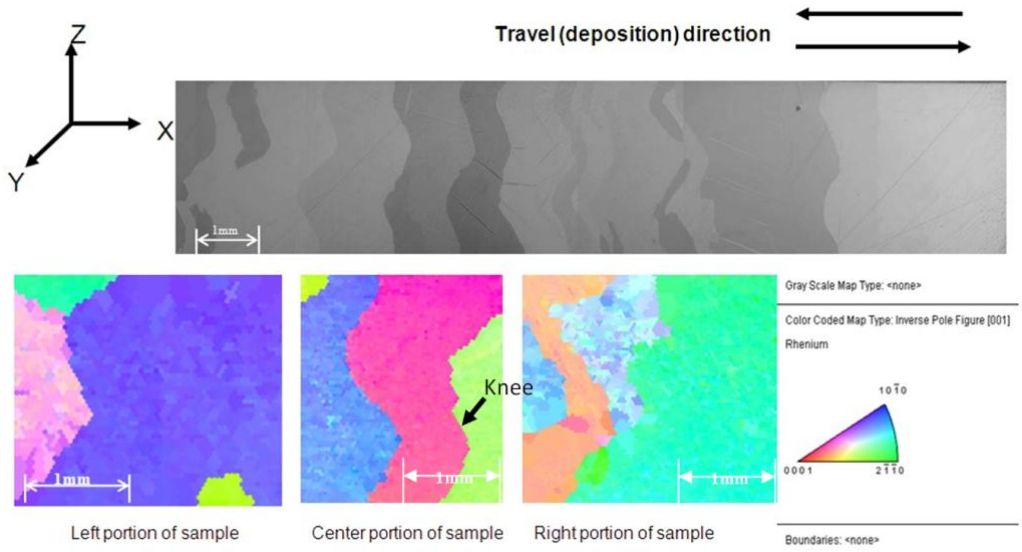

Figure 16. Compare the representative microstructure of the X-Z plane and representative crystal orientation for the X-Z plan to Figure 10.

Nanoindentation

Re mechanical properties can be heavily influenced by microstructure, thus an exploration of Re properties related to microstructure and crystallographic properties is in order. Nanoindentation is an indentation testing system that uses a very small, very precise indenter attached to sensors that record depth and load. These results are then analyzed by the system to deduce a variety of data such as hardness, Young's modulus, etc.[58, 59] The elastic stiffness of the contact, S, is related to the change in the load with change in displacement during unloading.

$$E_r = \frac{\sqrt{\pi}}{2\beta}\frac{S}{\sqrt{A}}$$

The variables are as follows: S is elastic unloading stiffness and is dP/dh, E_r is the reduced modulus, β is the indenter geometry factor and A is the projected contact area under load of the indenter. For a Berkovitch indenter (i), as used in the MTS Nanoinstruments Nanoindenter XP, β is 1.034. E_r is then related to E_i and $E_{test\ material}$ below where E and ν are the elastic modulus and Poisson's ratio of the material tested and E_i is the modulus of the indenter and ν_i is Poisson's ratio of the indenter.

$$\frac{1}{E_r} = \frac{1-\nu^2}{E} + \frac{1-\nu_i^2}{E_i}$$

The MTS unit imposes an oscillating load on the indenter. This is used to calculate a continuously measured elastic constant, S, noted below. Then Young's modulus is calculated as above.

$$S = \left[\frac{1}{\frac{P_{OS}}{h(\omega)} \cos ø - (K_S - m\omega^2)} - K_f^{-1} \right]^{-1} \qquad \omega\, C = \frac{P_{os}}{h(\omega)} \sin(\phi)$$

The variables are as follows[59]: S is elastic stiffness of the contact from the continuously varied load, P_0 is excitation amplitude, ø is phase angle, h is displacement, K_s is stiffness of the support springs supporting the indenter, K_f is load-frame stiffness, m is mass of indenter, ω is excitation frequency, C is damping coefficient of frame.

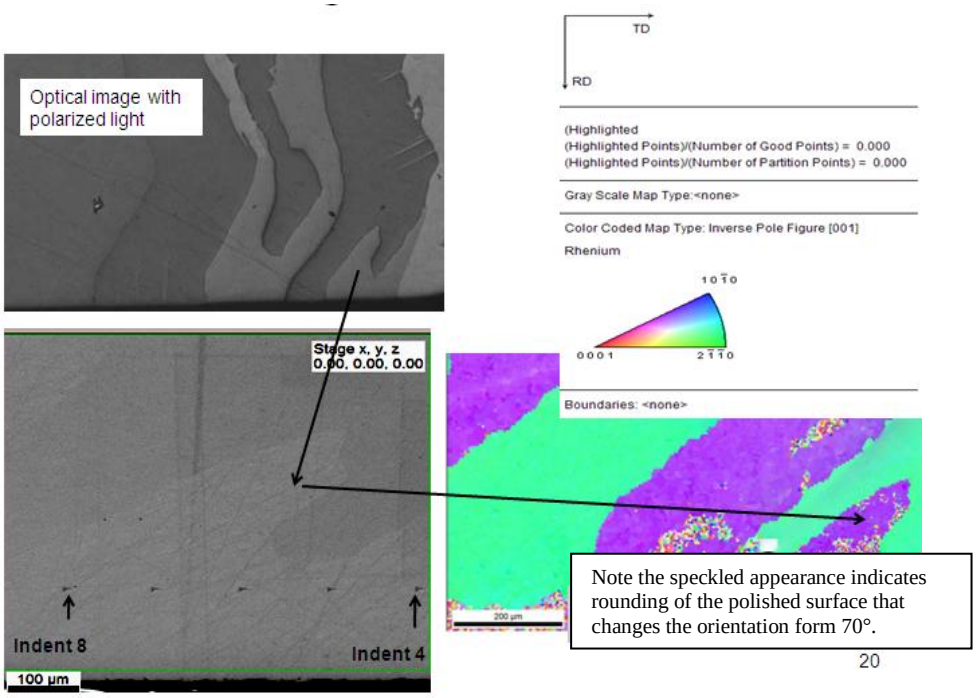

Figure 17. Comparisons of metallographic, OIM matching crystal orientation and a SEM photograph of same segment.

Young's modulus has been calculated from OIM crystallographic data for selected grains. The lower and higher moduli as measured by nanoindentation were selected for OIM measurement and moduli calculation. The calculated value of Young's

modulus compared to the nanoindentation measured values differs 5 to 21 percent relative to the calculated values. The calculated moduli differed from the bulk modulus from 0 percent to 7 percent. However, the entire range of seventy-eight nanoindentation values had a standard deviation of approximately 5 percent. If the standard deviation is taken into account, the calculated values are very close to the measured values. See Figure 18 for a graphical representation.

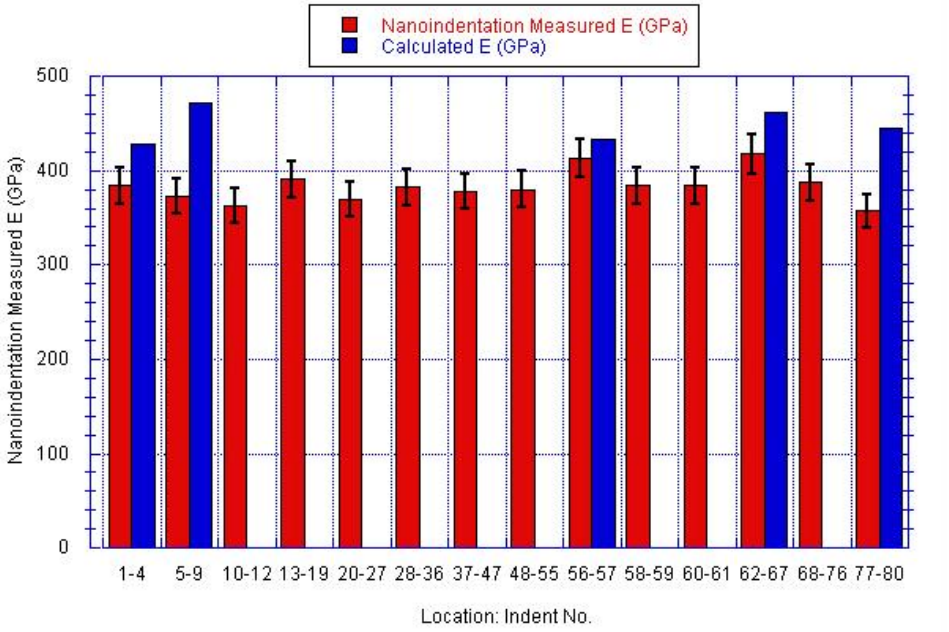

Figure 18. Comparison of nanoindentation measured Young's modulus and values calculated to date for Re. Error bars are shown depicting the standard deviation for all 78 nanoindentation measurements.

Tensile Testing

Materials and Experimental Procedure

Re plate was received and sectioned as shown in Figure 19. Ultra-high temperature (≥ 1371 °C) testing facility availability is limited and, as a result, bulk tensile testing took place in two locations: Southern Research Institute (SORI) in Birmingham, Alabama, and at Honeywell in Tempe, Arizona. The early testing was conducted at SORI

due to unavailability of the appropriate equipment locally. SORI used carbon tooling for the tensile testing load train in contrast to Honeywell, which used W tooling. See Figure 20.

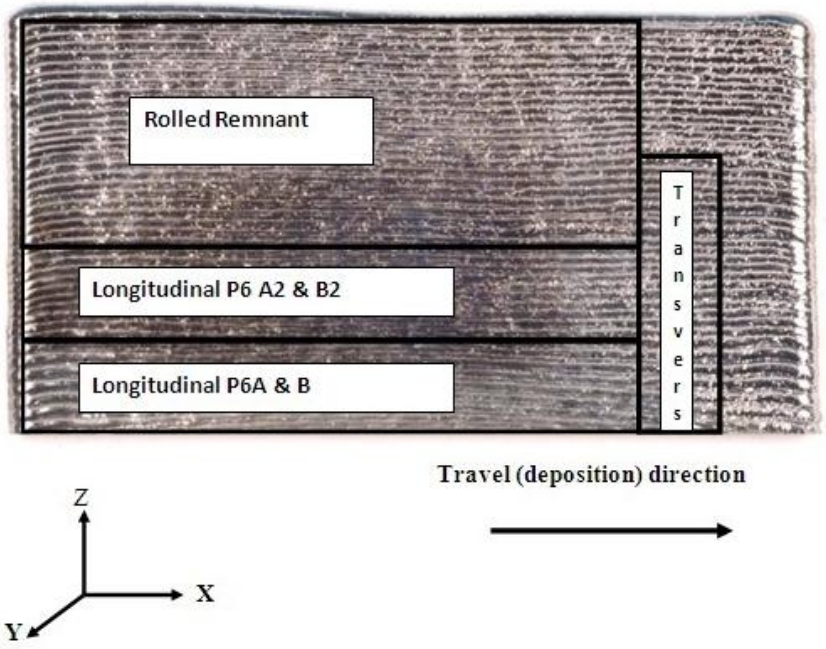

Figure 19. Sample locations for mechanical property testing of pure Re.

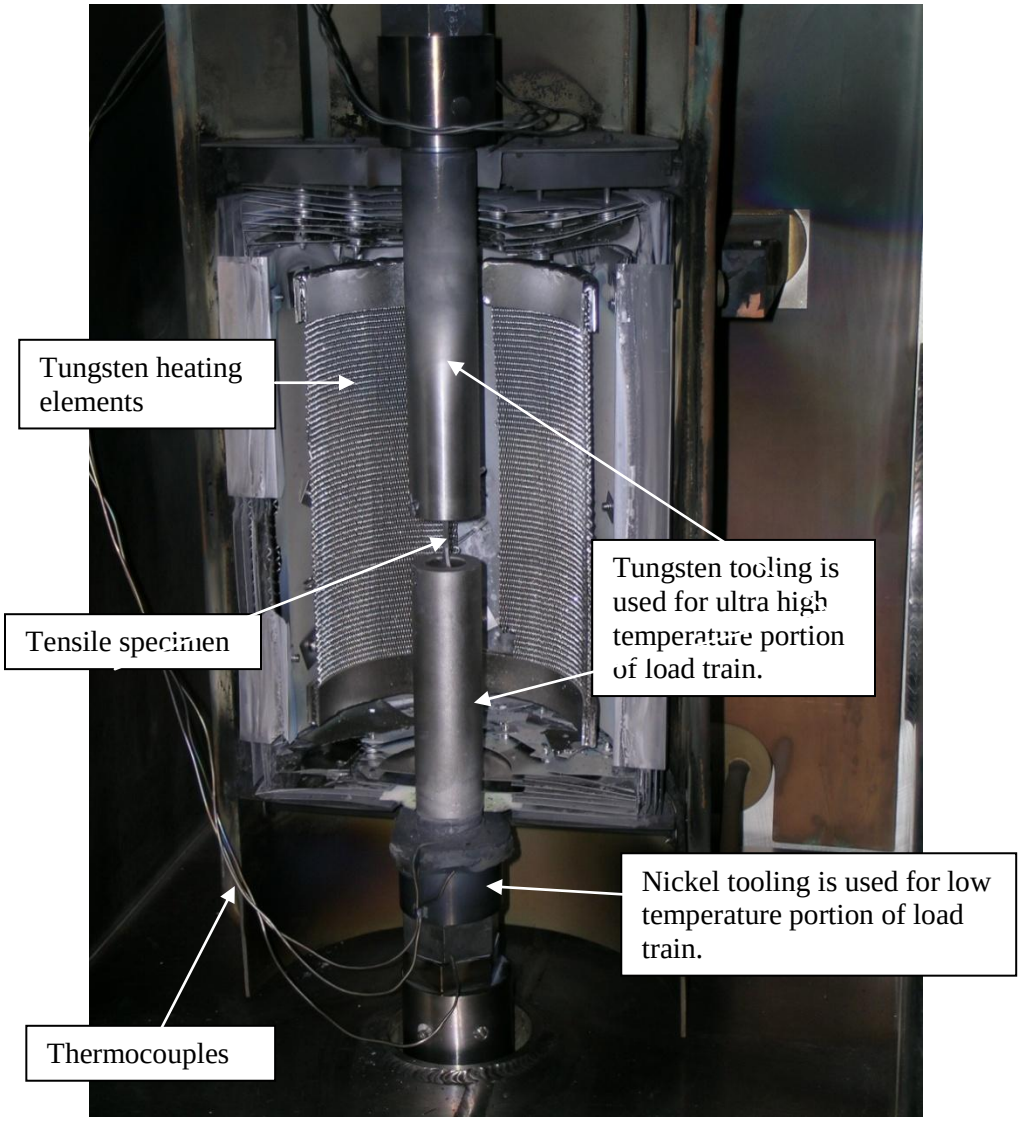

Figure 20. High temperature furnace and load train.

The author designed and sized the latter. Details of stress calculations are contained in Appendix A. As noted above the Re plate is shown in Figure 19 and depicts the location of tensile specimens in the pure Re plate. The 7.62 mm thickness of the Re plate allowed extraction of two approximately 3.5 mm thick blanks. Thus each planar location shown in Figure 19 represents two specimens designated as A and B. P in the sample number designate plate and the number immediately following indicates which

plate. The letter, “T” if present, indicates a specimen cut transverse to the deposition direction but parallel to the build direction. See Figure 21. It should be noted that inadvertently all specimens parallel to the travel direction were tested at SORI and those transverse to the build direction were tested at Honeywell.

Tensile testing at ultra-high temperatures almost always has custom procedures associated with it but, where possible, the steps described in ASTM E21 “Standard Test Methods for Elevated Temperature Tension Tests of Metallic Materials” were followed.

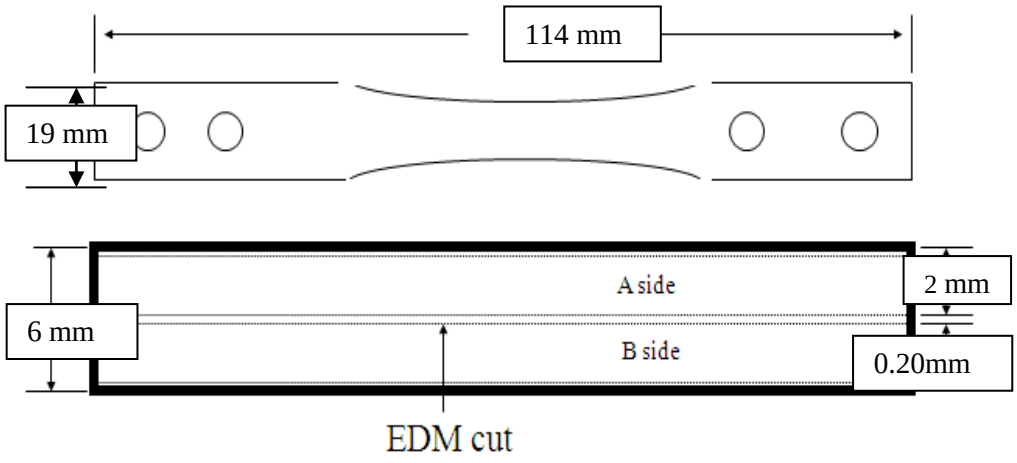

Figure 21. Schematic of SORI tensile specimen and view of location within the LAM plate prior to extraction.

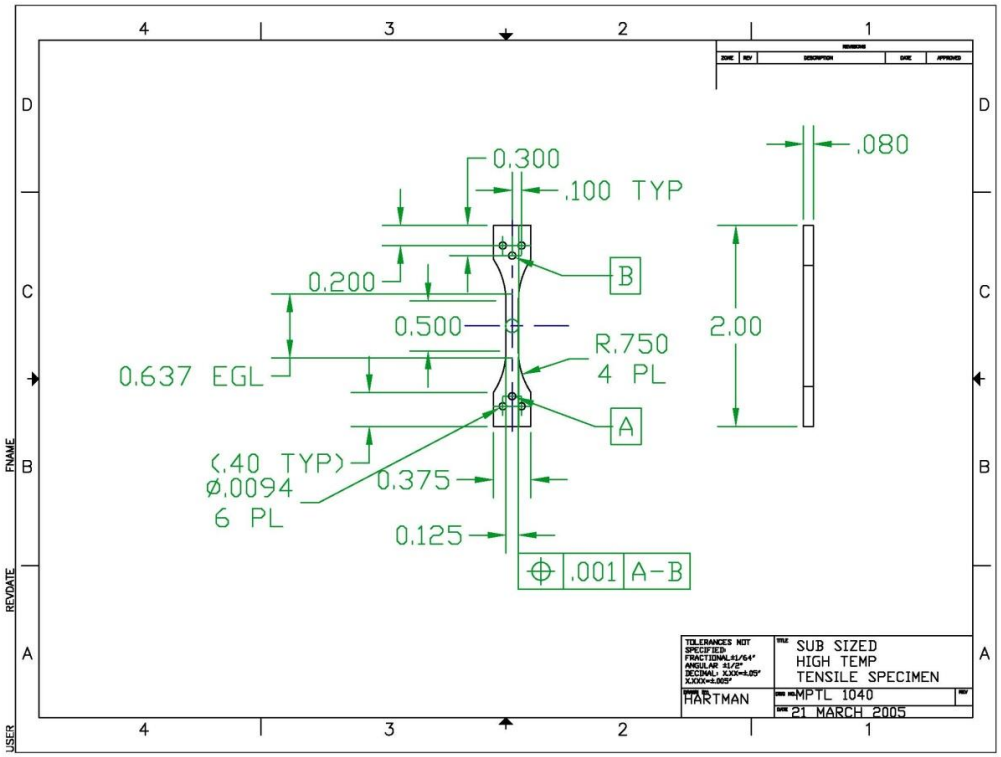

Figure 22. Honeywell tensile specimen drawing used for ultra-high temperature testing.

SORI has contact extensometers and is able to record strain data and calculate yield stress. Honeywell records crosshead movement and cannot determine yield stress. In the latter case tooling compliance is first measured with a large W bar connecting the entire tooling train. The load train is then loaded and displacement vs. load is recorded. This is then subtracted from the actual test data to give valid specimen strain. See Figure 23.

Results and Discussions

Mechanical tests at elevated temperatures of 137 °C and 1925 °C revealed significant differences for pure Re with respect to the properties reported in the literature for powder metallurgical samples. Typically, the latter have elongation at these elevated temperatures below 5 percent and sometimes a fraction of a percent.[38-40] Tests of LAM Re at elevated

temperature have revealed elongation ranging from 14 percent to 26 percent. For elevated and ultra-high temperature structural applications, this is a significant improvement in properties. Unfortunately, the strength was reduced compared to that noted in the literature for other fabrication properties. Table 11 shows the SORI results. The graph, Figure 23, shows strain to failure whereas the table lists strain at maximum stress and strain at fracture. Subsequent to the SORI tests additional tests were performed at Honeywell using W tooling. The samples were parallel to the build direction i.e. perpendicular to the travel direction and the axis of the SORI tested specimens. Similar results were found except one Honeywell tested specimen had slightly lower strength. Insufficient specimens were tested to prove a definite trend. See the results in Table 12 and Figure 24. The latter figure shows the as-tested data and the corrected data after subtracting strains from compliance testing.

Table 11.Tensile Data Provided by Southern Research Inc. Using Carbon Tooling.

Specimen	Test Temperature (°C)	UTS (MPa)	0.2 percent Offset Yield (MPa)	Strain at Max. Stress (percent)	Strain at Fracture (percent)
Tn-P6-B1	1371	228	69	11	14
Tn-P6-A2	1371	220	58	19	22
Tn-P6-A1	1925	89	40	12	23
Tn-P6-B2	1925	62	30	13	26

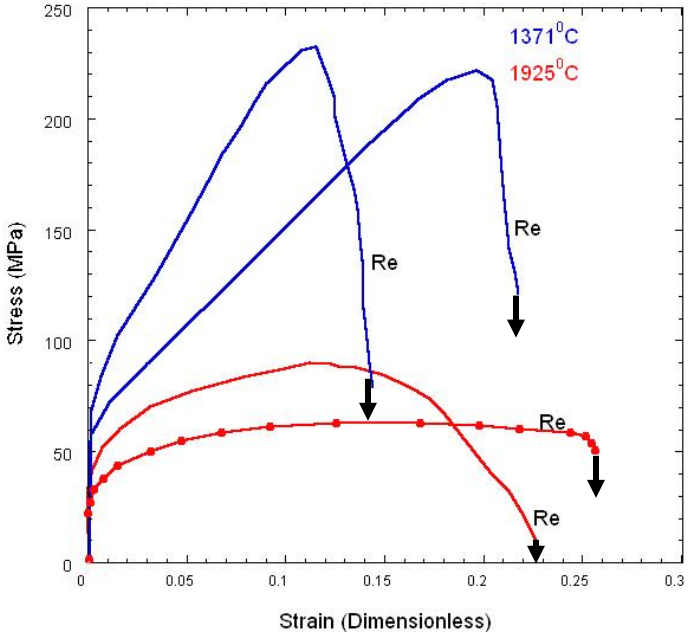

Figure 23. LAM pure Re strength and strain to failure tested at SORI properties of pure Re.

Table 12. Pure Re Transverse Tensile Tests at 1925 °C Performed at Honeywell.

Specimens	**UTS MPa**	**Total Elongation (percent)**
P6T1	62	16
P6T2	45	16

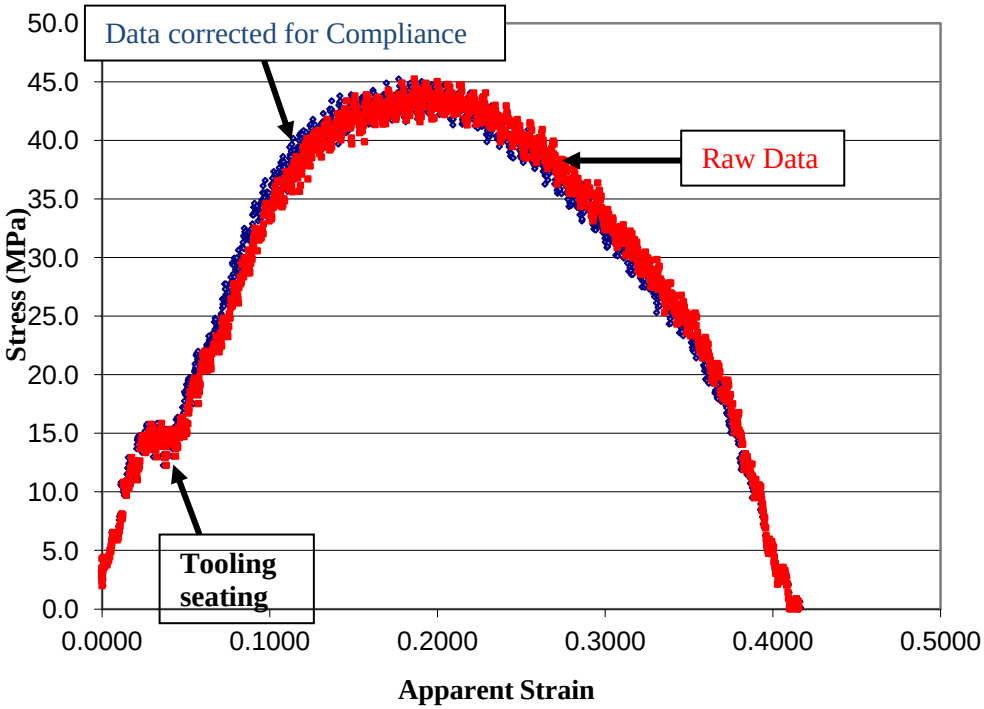

Figure 24. Graphical representation of stress vs. apparent strain seen in pure Re when tested at 1925 °C for specimen P6T2.

Fatigue Testing

Materials and Experimental Procedure

Only one pure Re plate was delivered. After tensile specimens were extracted, insufficient material remained for complete fatigue samples. To enable fatigue testing wrought material was added to the ends of the gauge section ends using electron beam welding. The grip ends were sufficiently removed from the gauge section that they did not affect the test results. See Figure 25.

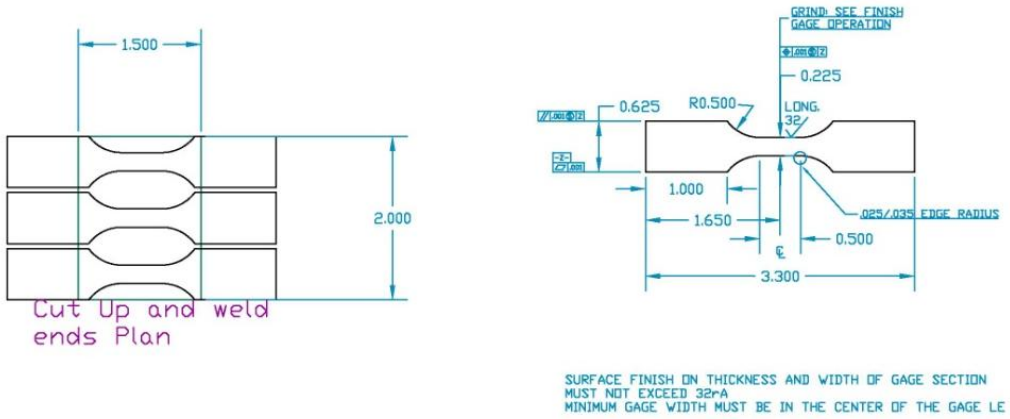

Figure 25. Welded fatigue specimens.

Six samples were cycled under load control at room temperature. R was 0.1 and the frequency was 15 hertz although there was a slight deviation to 40 hertz for one specimen. See Table 13. The tests were tension-tension as the specimens were too thin to run in compression. Noticeable deformation, visible to the eye, was noted in the early stages of the first test.

After the first test when so much deformation was visible, a monotonic test was performed and stress strain data for the first cycle of the next two tests was collected. The sample was loaded in 5 seconds to the mean stress for that sample and the load-strain data recorded for that cycle and the following 100 cycles. The same data was then recorded periodically for subsequent cycles.

Results and Discussion

There was insufficient material available to be able to construct a stress vs. life (SN) curve. However interesting trends appear that bear further investigation if more material becomes available. Applying a stress transverse to the build direction (transverse to the grain and parallel to the deposition travel direction) tends to result in a shorter life

than the same stress applied parallel to the build direction. Additional work is required to verify if this trend is valid or an anomaly.

Table 13. Fatigue Test Results.

Sample No.	Test Temperature	Orientation	Load (MPa)	Cycles to Failure	R	Frequency (Hz)
1042-1-6	RT	Axial	152	15,347,586	.1	40
1042-2-6	RT	Axial	207	1,184,694	.1	15
1042-2-5	RT	Transverse	207	738	.1	15
1042-1-5	RT	Transverse	125	6,331,991	.1	15
1033-1	RT	Transverse	180	6,664,656	.1	15
1033-2	RT	Transverse	207	103,261	.1	15

Axial: Grain axis is parallel to specimen axis and parallel to build direction.

Transverse: Grain axis is transverse to specimen axis and specimen axis is parallel to travel direction but transverse to build direction.

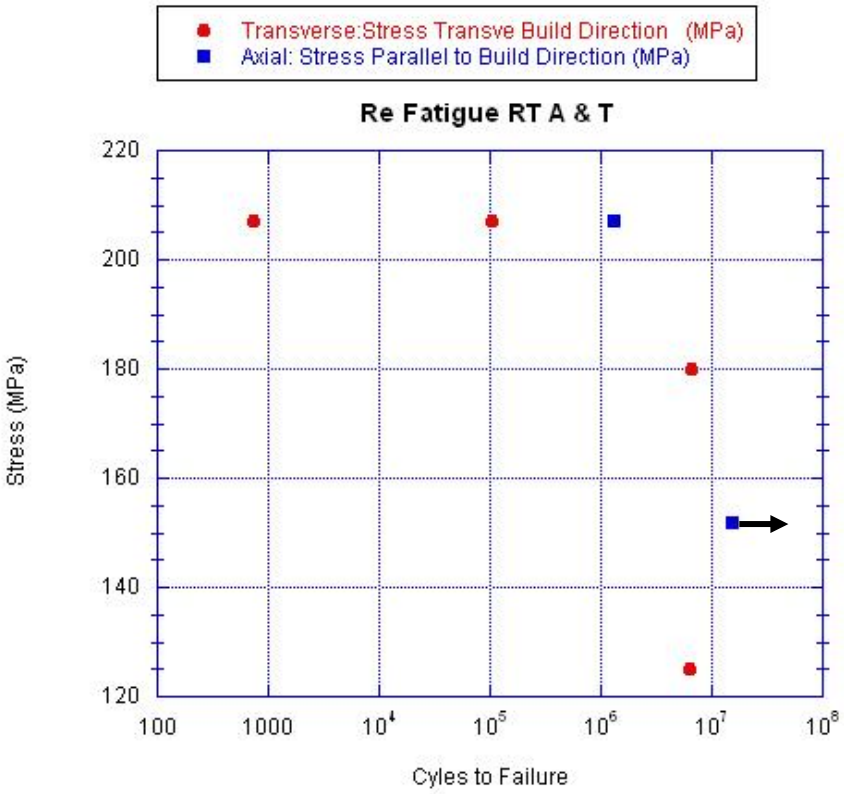

Figure 26.Plot of fatigue results from Table 12 for pure Re.

One aspect of interest when conducting a fatigue test is the strain hardening. That is the increase of flow stress with increasing numbers of cycles when in strain control testing.[65] This is noticeable even in the early cycles but eventually stabilizes to a constant as the test progress. The latter state is called saturation. When fatigue testing in stress control, saturation can be noticed as strain diminishes with constant stress amplitude. As-deposited LAM Re is very soft and the test conditions must take this into account, as will be shown shortly. In the first fatigue test the machine continuously shut down due to exceeding deflection limits. At the start of the second test, as previously mentioned, during the first cycle stress vs. strain was continuously recorded and a stress-strain curve was created up to the maximum load of the test. The curve created included the elastic portion of the curve and the beginning portion of the plastic portion. See Figure 27.

Strain hardening was observed in two ways in this test. The first is smaller hysteresis cycles in a plot of cyclic stress vs. cyclic strain and the second was a plot of strain vs. time. Examination of the hysteresis curves indicate a narrowing of the space between increasing tension and decreasing tension as the number of cycles increase. In Figure 28 the hysteresis narrows from 0.0004 mm/mm to 0.00029 mm/mm for a decrease of 28 percent strain per cycle. In Figure 29 the strain per cycle is reduced with time.

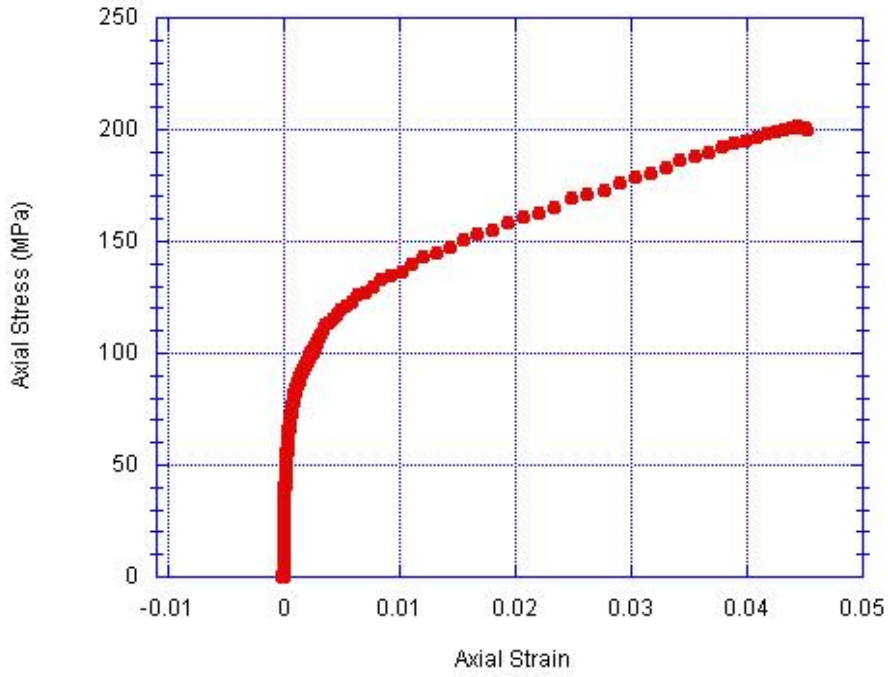

Figure 27. Stress strain curve from first cycle of RT fatigue of pure LAM Re specimen 1042-2-5.

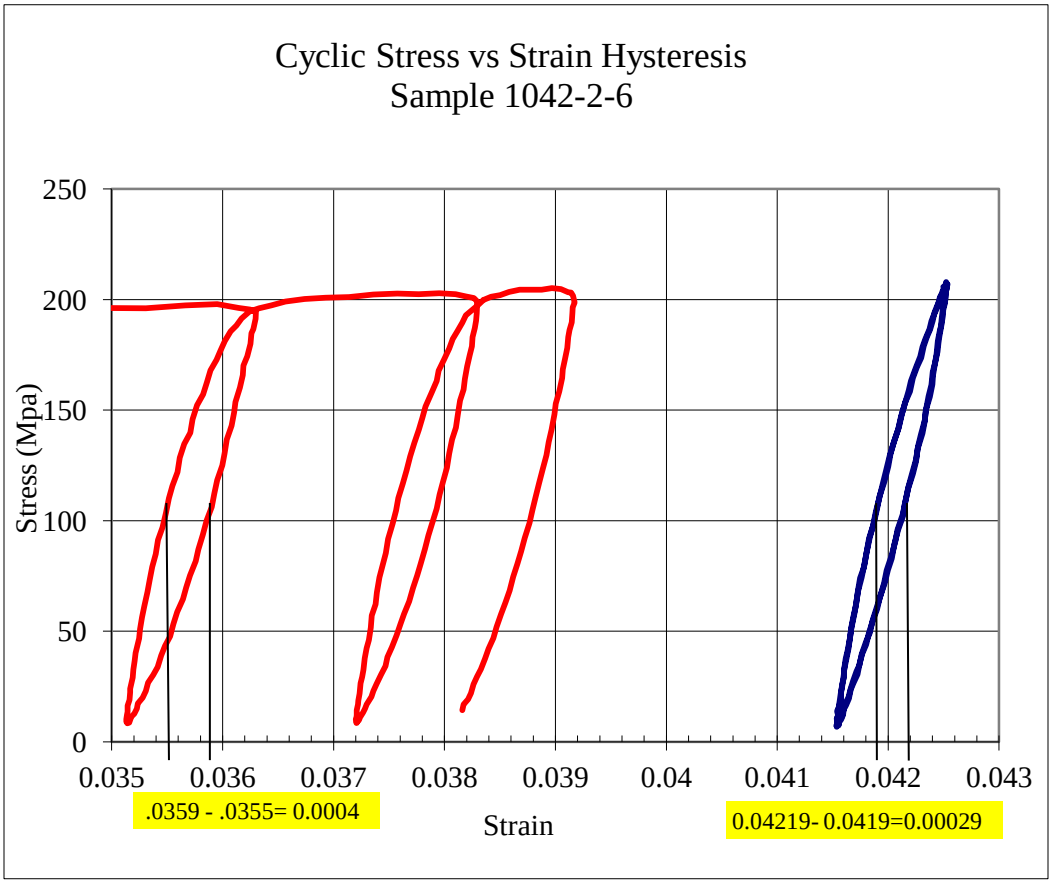

Figure 28. Graphical representation of stress vs. apparent strain cyclic hysteresis is seen in pure Re sample 1042-2-6 when tested at RT at various cycles. Note the change in width of the hysteresis loop. The smaller width in the later loop may indicate strain hardening.

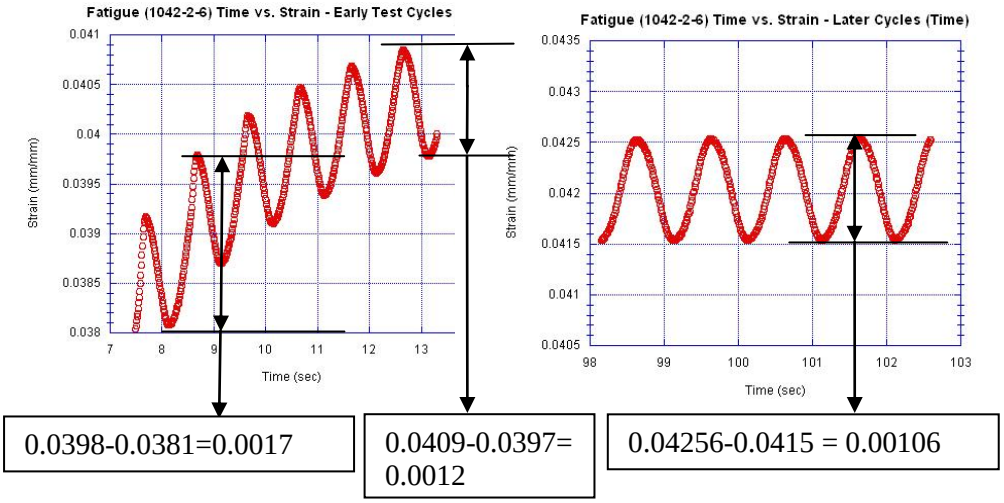

Figure 29. Evidence of strain hardening due to fatigue cycling is shown by the valley to peak distances. Note in the early cycles the total strain is increasing.

Fractography of Tensile and Fatigue Specimens Using Electron Microscopy

Materials and Experimental Procedure

Electron microscopy examination of the fractured specimens was undertaken to better understand the fracture mode of this form of Re. Scanning electron microscopes at ASU LeRoy Eyring Center for Solid State Science, ASU Materials Mechanical Test Laboratory and the Honeywell Materials Laboratory in Phoenix were used.

Results and Discussion

Tensile Fractography

The predominant tensile fracture mode of Re at room temperature is intergranular due to limited slip systems. At elevated temperature LAM Re has a variety of fracture features ranging from dimples to flat facets or even smooth surfaces as noted in Figure 30. The dimples noted at 1371 °C agree with the features found by Biaglow and Chazen.[31, 32] No record of fracture at ultra-high temperatures i.e. above 1371 °C was found in the open literature. Scanning electron microscope examination of tensile fracture faces for specimens parallel and transverse to the build direction exhibited very smooth

features. They are exhibited in Figure 30 and Figure 31 and Figure 32.These changes may be indicative of deformation and fracture mode changes as temperature varies.

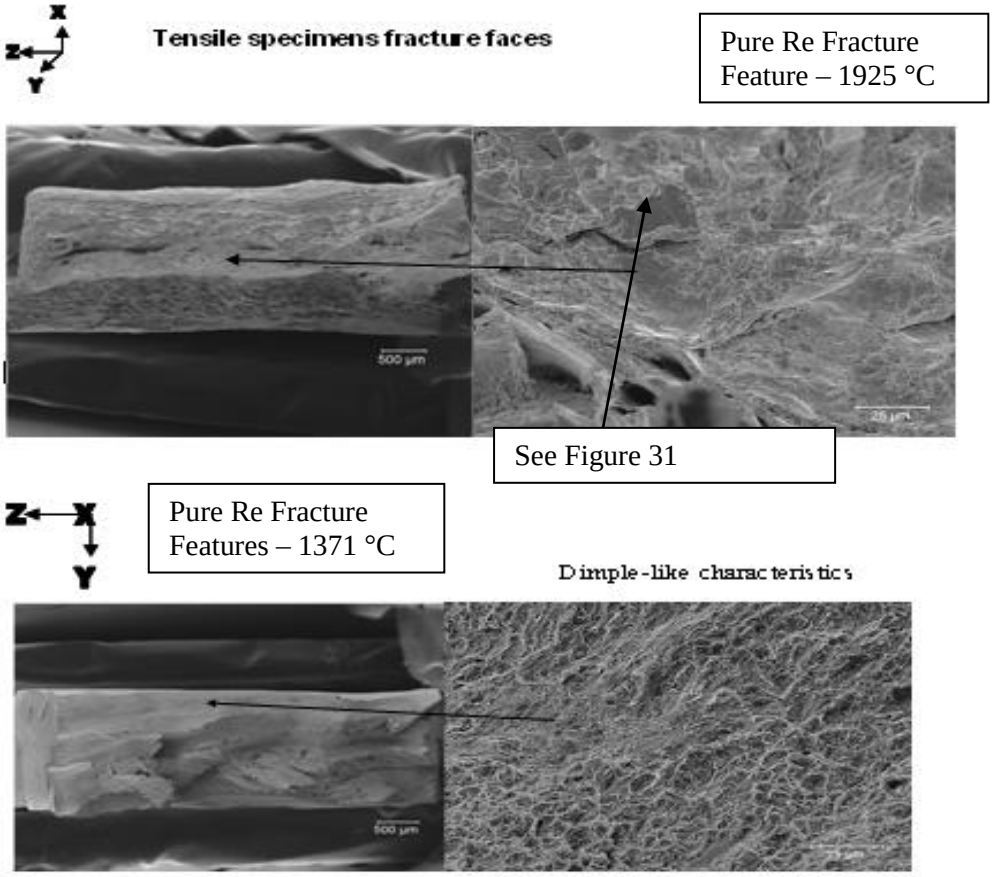

Figure 30. Micrograph of pure LAM Re fracture features tested at 1925 °C and at 1371 °C respectively.

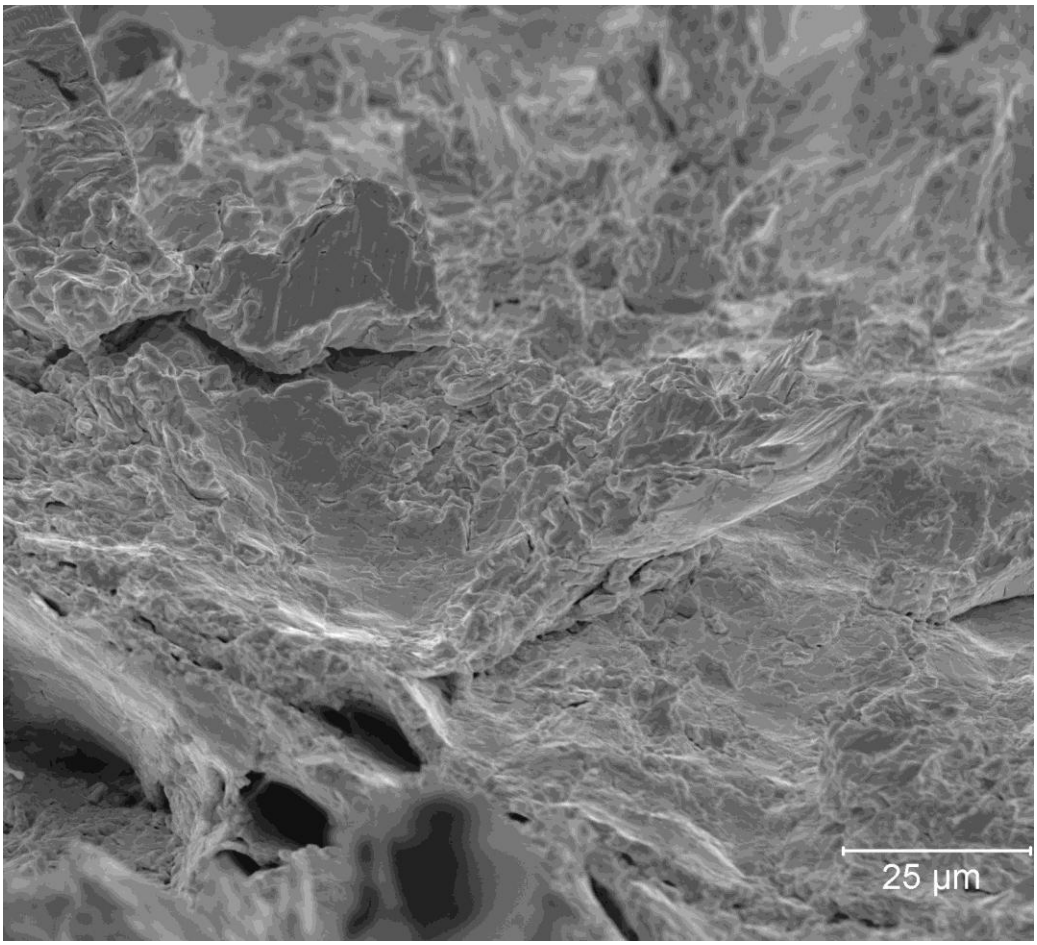

Figure 31. Enlargement of Figure 30 shows the smooth surfaces of finer features of the fracture when tested at 1925 °C, especially noticeable at left side of photograph.

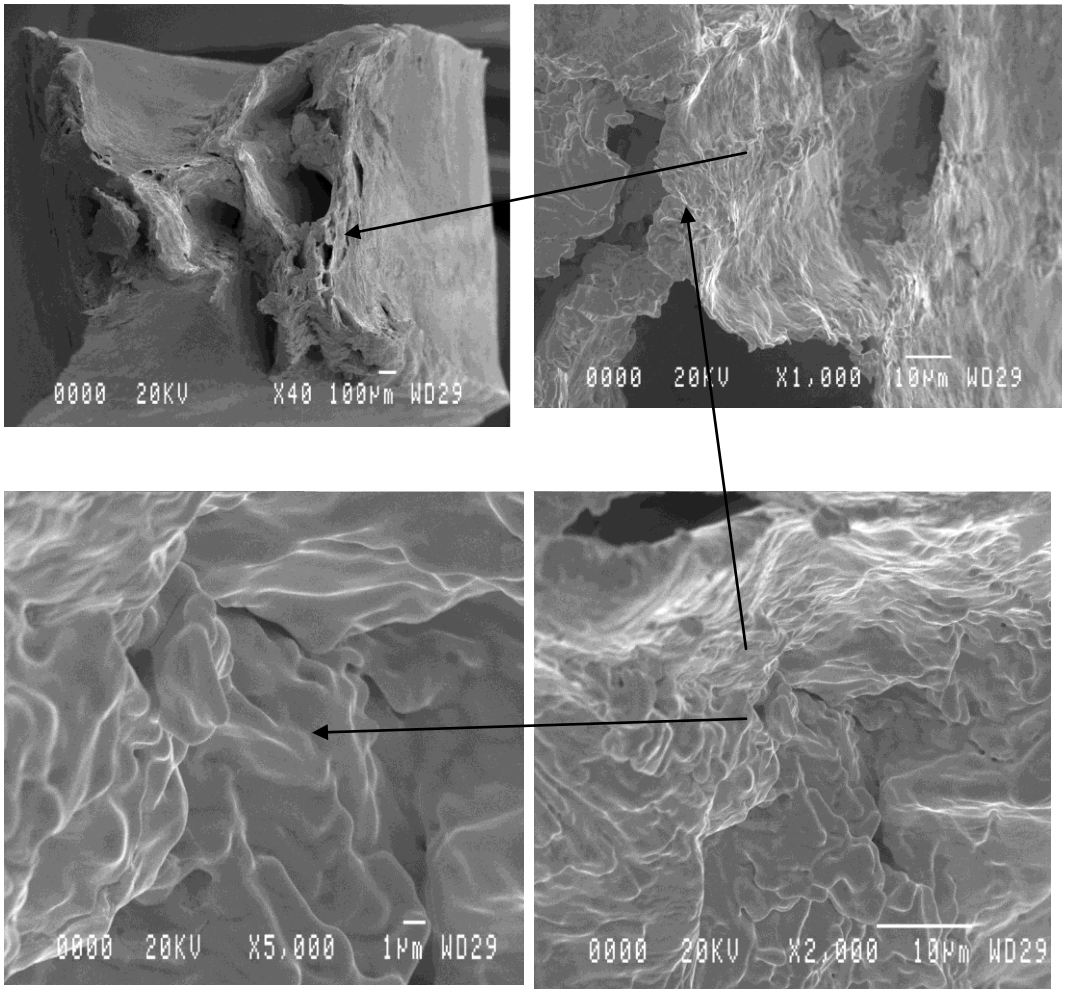

Figure 32. Tensile fracture features found at 1925 °C.

Fatigue Fractography

Fatigue fracture feature description was only found in Chazen where he described an intergranular fracture mode with striations that occurred when tested at high temperature (1371 °C) in fatigue. The fatigue fracture features of the axial samples whose specimen axes were parallel to the build direction exhibited a layered stringy appearance. See Figure 33, Figure 34 and Figure 35. Fracture features of the fatigue samples whose axes were transverse to the build direction and parallel to the deposition direction had a

macro-appearance that was smooth with undulations along the surface. Deformation resulting from the stress applied during the test highlighted the grain boundaries and showed them transverse to the specimen axis. See Figure 36 and especially Figure 37. At very high magnification, thin surface lines are seen that may be striations. The distance between striations is approximately 1 micron. In addition, rough stringy layered areas with steps were found that were most likely tears of islands not fractured by fatigue propagation. The undulations may be grain boundaries where dislocations accumulated similar to the intergranular fracture mode found in room temperature tensile fracture features. See Figure 38 and Figure 39.

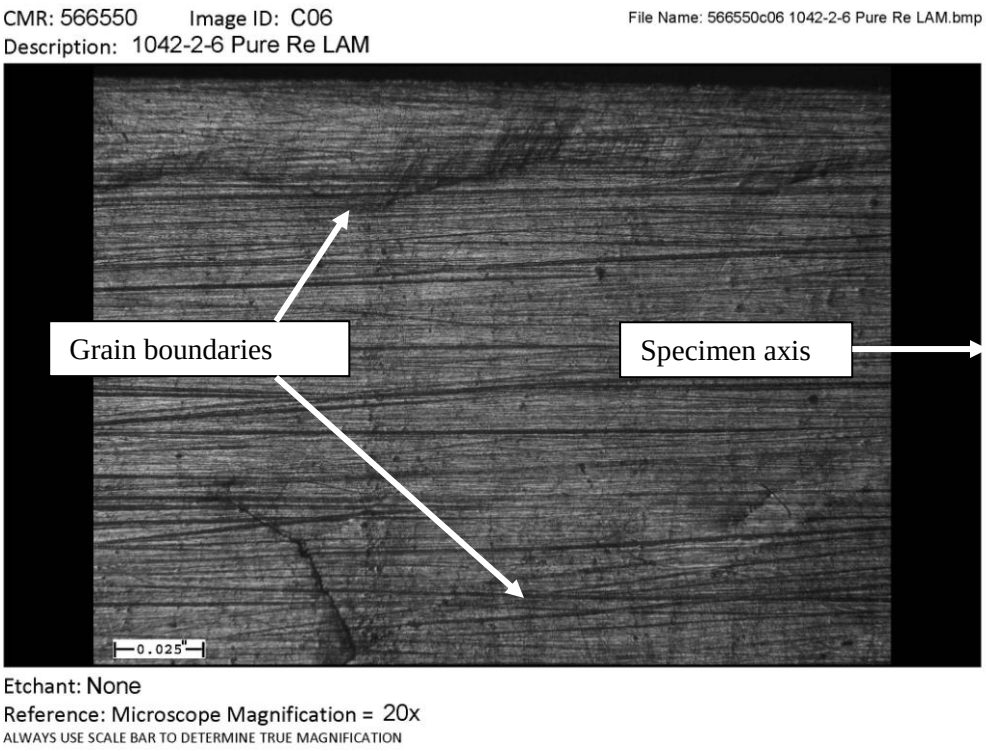

Figure 33. Photomicrograph shows grain morphology of fatigue specimen 1042-2-6 after completion of test. Deformation from test shows grain relief. Note grains are roughly parallel to fatigue specimen axis.

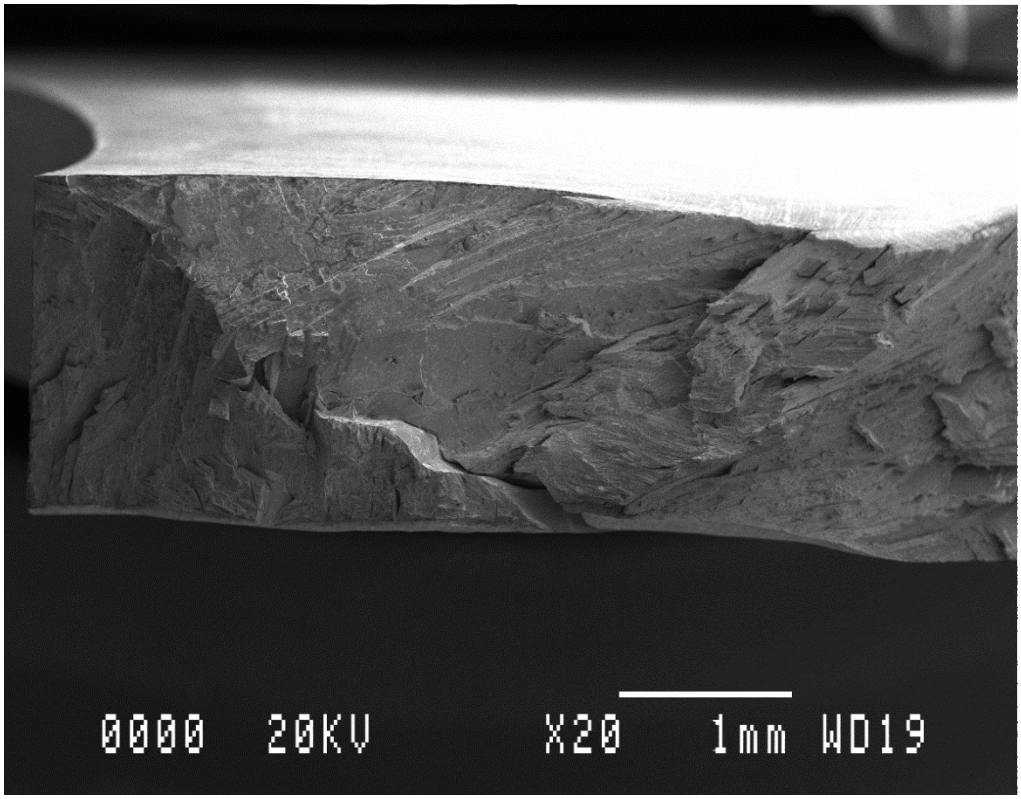

Figure 34. Overview of specimen 1042-2-6 with the specimen axis transverse to the deposition (travel) direction but parallel to the build direction labeled axial. Note the very different fracture morphology than the subsequent transverse specimens.

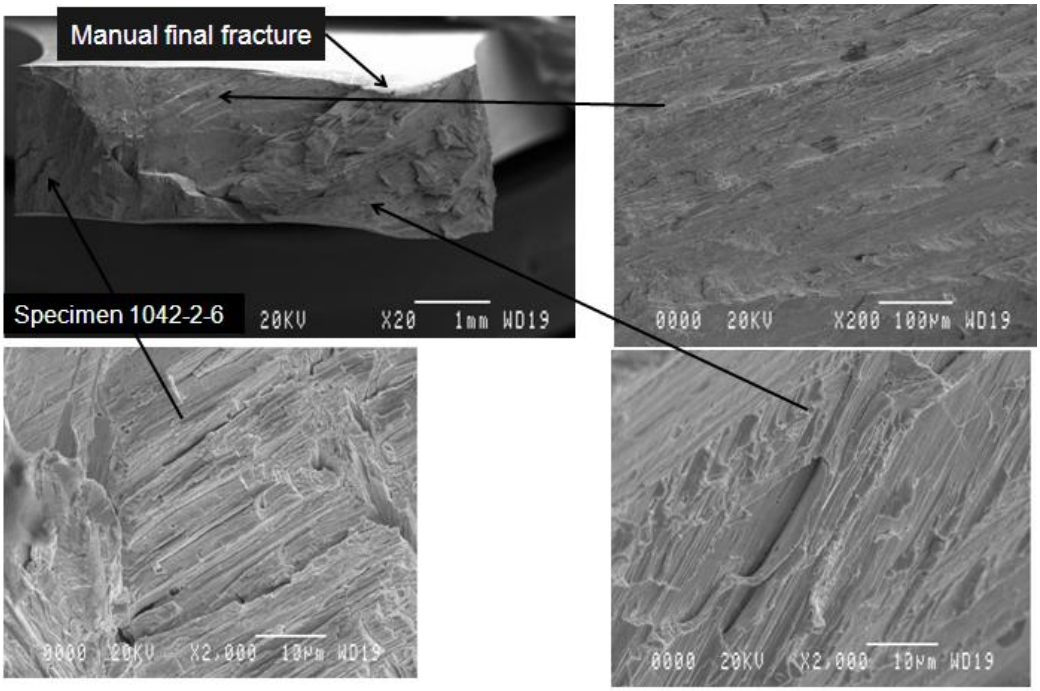

Figure 35. Fracture features showing probable tearing features resulting from fatigue stress transverse to the specimen axis and the elongated columnar grains in fatigue specimen 1042-2-6.

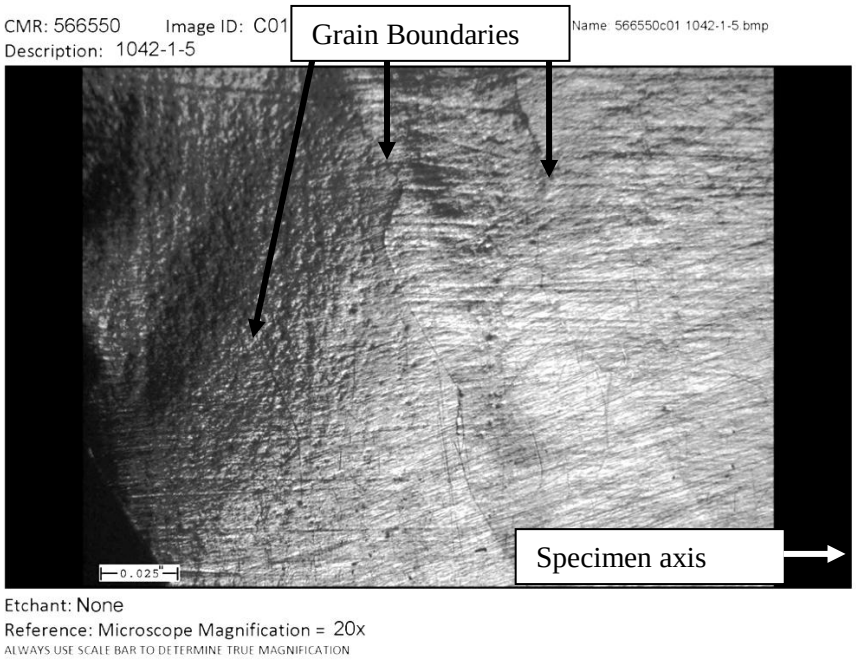

Figure 36. Optical picture at fracture showing orientation of grain shape as transverse to 1042-1-5 specimen axis but parallel to build direction.

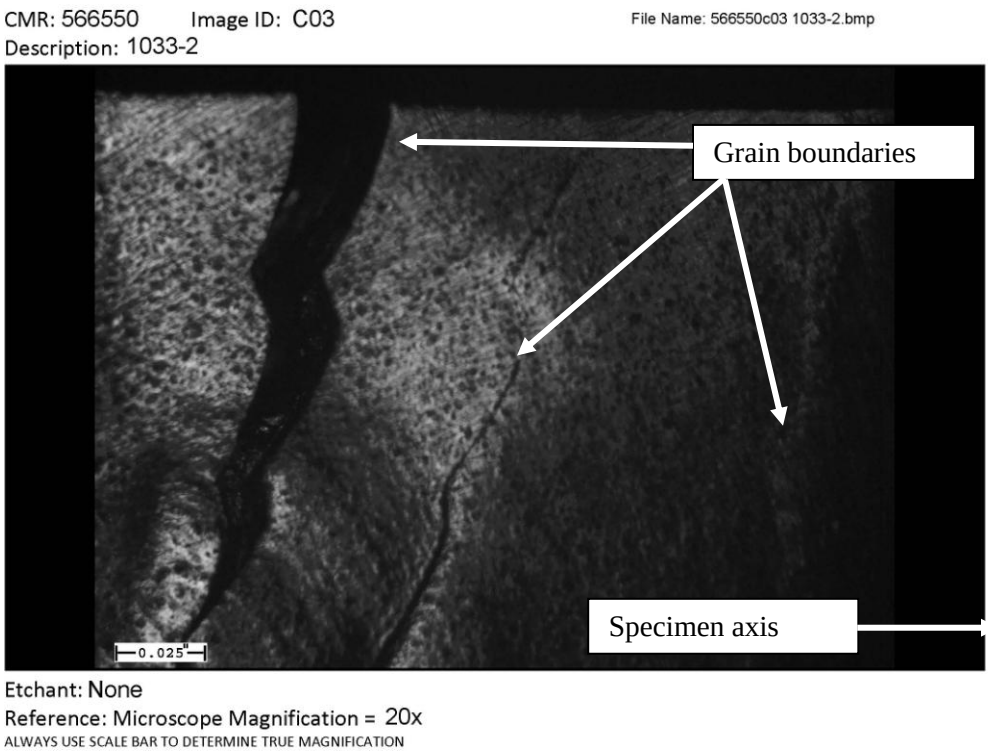

Figure 37. Optical photograph shows fracture of specimen 1033-2 with a more obvious fracture at the grain boundary.

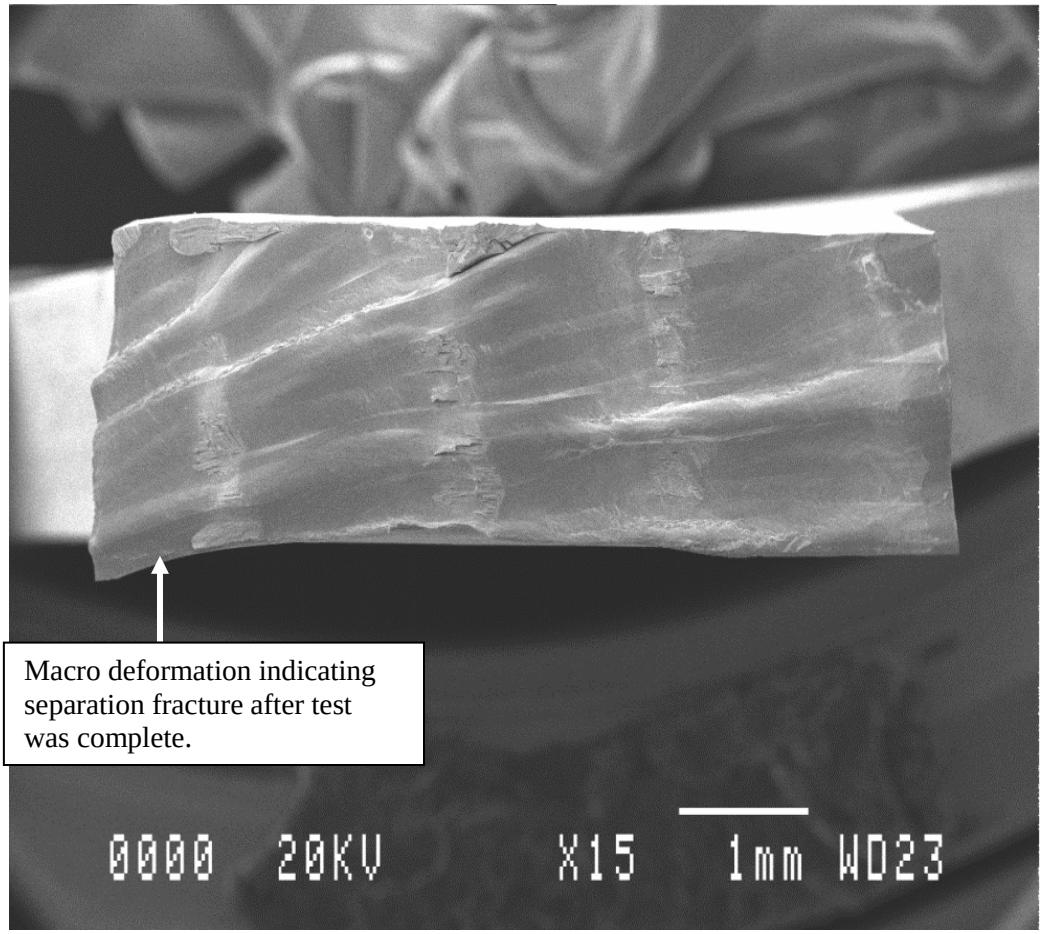

Figure 38. Note undulating fracture surface of specimen 1042-1-5. See Figure 39. Note that this specimen axis was transverse to the grain axis.

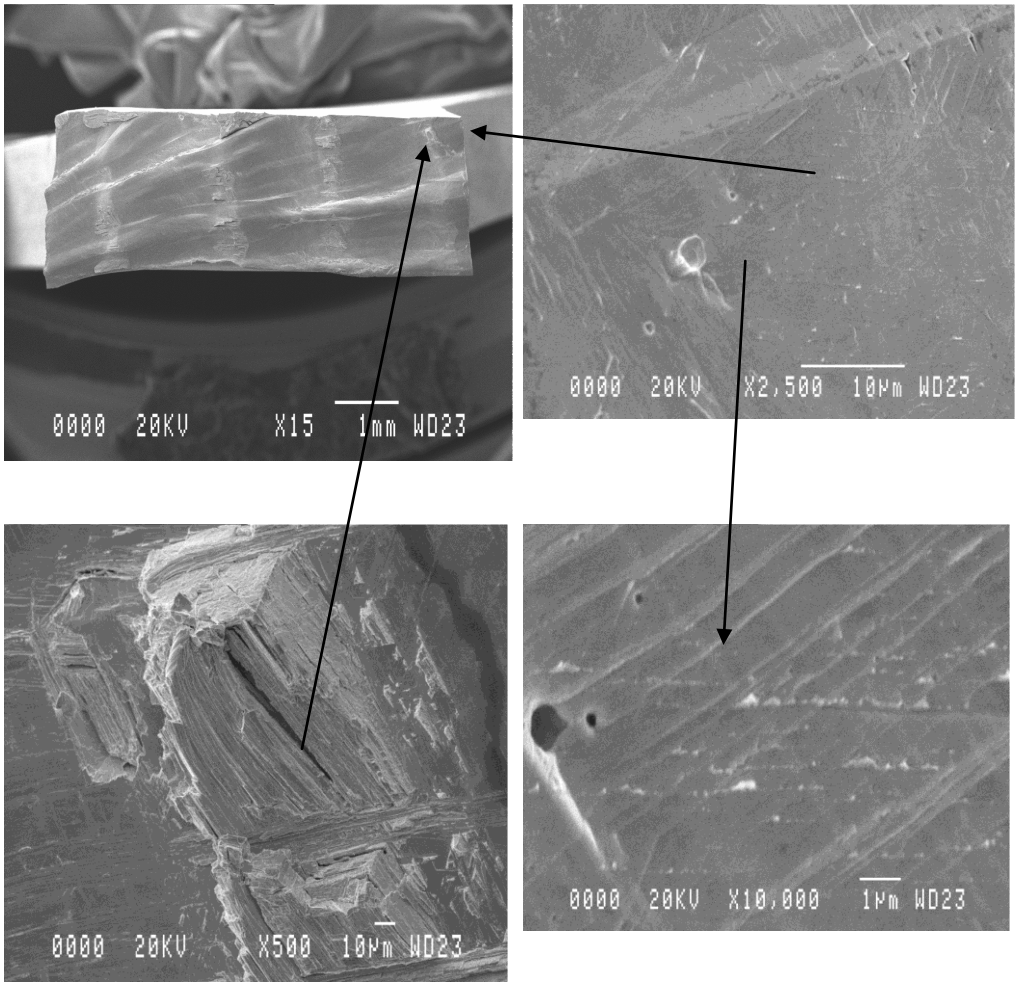

Figure 39. Fatigue fracture surface of specimen 1042-1-5. Note the fine ridges in the lower left picture. They appear to be striations.

Discussion

Many interesting trends have been found with the work to date. The first is the high ductility of pure LAM rhenium at elevated temperature compared to conventionally processed material. See Table 6 and Table 7. LAM Re exhibits high ductility, approaching or exceeding 20 percent elongation, at elevated temperature compared to the typical values, some as low as <1 percent, exhibited in other Re forms when tested at elevated temperature. See Table 11 and Table 12 and Figure 23. The elongation at failure

exceeds other Re forms in some cases by more than a factor of 20. This high ductility compares favorably to single crystal ductility although lower. Such improvement may result from a change of deformation mechanism or from an absence of impurities. The latter could be vaporized and perhaps eliminated by the high temperature of the molten puddle, greater than 3180 °C, during deposition. Additional work will be required to resolve this issue.

The grains are very large and extend across deposition layers, a common occurrence in AM. They are large enough to allow significant movement of dislocations within a given grain and could contribute to enhanced ductility. While the grain envelope axis is roughly vertical to the deposition layer plane, they have a slight tilt relative to vertical that is influenced by direction of travel.

The work done to date opens the possibly of property improvement. Addition of other materials, usually other metals, can improve attributes of pure metals.[33, 34, 35] Several effects result. One common method of improving strength is to reduce the grain size. This could be effective, since pure LAM Re has such large grains. Materials that enter into a solid solution often can increase strength or make improvements to other attributes such as oxidation resistance. The matrix material is called the solvent and the added material is the solute. In a substitution solid solution, the solute material takes the place of solvent atoms. The solute will be either larger or smaller than the matrix atoms. In either case, internal stresses are created that impede dislocation movement and strength may increase. If the solute atoms are sufficiently smaller then the matrix atoms they may be able to fit into the spaces between the atoms, the interstitial sites. Such interstitial solutions can also increase strength.

In some cases, the solute is soluble in the solvent at elevated temperatures but tends to combine chemically with other elements to create small particles as temperature decreases. Typically those particles are not soluble in the solvent and precipitate out of solution. They can also impede dislocation movement and as a result increase strength. Strengthening of this sort is called precipitation hardening. Another strengthening approach is to introduce very small particles called dispersoids that have no solubility in the solvent. They also impede dislocation movement and can increase strength. This technique is called dispersion hardening.

Study of Re alloys is limited but some precedent exists for developing Re alloys and possibly improving properties. Alloying with 4.5 per cent W was examined using LAM by AeroMet and tested by RAI.[67] The immediate effect was to reduce grain size relative to pure LAM Re but they are still somewhat large. The deposit had ultimate strength at 1371 °C ranging from, 192 MPa to 258 MPa with accompanying strain at maximum stress of .04 to .26. The lower strain at maximum stress occurs with longitudinal samples and higher values with transverse samples. These strength values are in the lower range of the conventional processes but about the same as the pure Re samples tested at 1371 °C.[67] In addition, Re alloys with better resistance to oxidation have been reported. [68] Thus modification of pure Re could improve its mechanical properties but significant work would be required.

Rhenium can present a significant challenge for OIM examination. Since the material work hardens so readily, it can easily have surface anomalies from disturbed surface layers even after extended polishing. These disturbed layers give a non-uniform pattern when examined with OIM. Careful examinations of resulting orientation maps typically reveal a dominant orientation. However some remain highly random. Only

indices from those maps that had clearly dominant orientation were used to calculate moduli in this report. In addition the grains were so large that most grains had more than one indentation and were averaged to produce one modulus number for that grain. OIM of the crystal orientation of the grains to date indicates a variety of orientations. Much more work is required to confirm this trend.

Nanoindentation measurement of Young's modulus of LAM Re to date varies from approximately 4 percent below the average bulk Young's modulus of 460 GPa to approximately 25 percent below that value. Calculations have shown Re modulus varies with direction so variation of one location from the bulk which is an average over many grains is reasonable. The nanoindentation loading graphs exhibit the classic theoretical shape expected. Both these facts indicate nanoindentation is a viable technique to evaluate Re properties.

Fracture modes for elevated temperature and ultra-high temperature tensile testing differ from each other and from the typical intergranular mode exhibited by room temperature Re fracture. Room temperature fracture is intergranular. At 1371 °C the fracture mode is dimple rupture but at ultra-high temperatures fracture features are very smooth with some undulations (ripples). This could very well be indicative of a deformation and fracture mechanism change. The fracture features of micro-void coalescence, also called dimple rupture, at 1371 °C match that found in the literature. However at ultra-high temperature the very smooth fracture features are most likely a shearing mechanism. In this failure mode, the planes with the least strength slide over each other until fracture is complete. The features most closely resemble glide–plane decohesion but examples available in the literature were only for room temperature fractures. No examples of fracture at ultra-high temperatures were found in the open

literature. The span between the proportional limit and the ultimate strength in LAM Re is related to the work hardening rate caused by the combination of limited slips systems found in hcp materials, dislocation intersections and generation of twins as discussed previously. On the other hand, the very high elongations at elevated temperature could result from very fast, if not instant, annealing at the test temperatures of 1371 °C and certainly at 1925 °C since the recrystallization temperature ranges from 1300 °C to 1500 °C. Dynamic annealing could result in reduced work hardening at elevated temperature.

Fatigue strength of pure LAM Re varied significantly revealing extremes of values. Many factors affect the fatigue strength of material and include the presence of precipitates, impurities inclusions, grain boundaries, crystal orientation, texture, etc.[33,34, 35, 66] Chemical analysis indicated pure LAM rhenium had very low levels of any elements other than Re. However LAM is essentially a computer controlled weld process. One of the more common defects from welding is lack of fusion. No evidence was found of this flaw type or any other common weld defects including the specimens with very low cyclic life.

Fatigue mechanisms are different from monotonic tensile fracture mechanisms but some lessons may be learned. At room temperature Re fails predominately with an intergranular fracture mode in monotonic testing due to differing crystal orientation. With only three slip systems the misorientation between grains can prevent dislocations from traversing from one grain to another, cause dislocation pile up at misoriented grain boundaries and result in micro-cracks. In fatigue a similar mechanism could occur. Persistent slip bands, associated with fatigue, can traverse low angle grain boundaries but are blocked by high angle boundaries. [66] Thus the same mechanism of grain boundary

pile-up leading to intergranular monotonic fracture mode could initiate fatigue fracture at grain boundaries. This fits one of the three requirements for fatigue initiation at grain boundaries i.e. adjacent grains are misoriented with respect to each other. The other two are the active slip system of at least one of the grains intersects a grain boundary and third, the grain boundaries must make a large angle, thirty to ninety degrees, with the tensile axis. It is safe to assume that at least one grain in the tested samples had at least one slip system directed at the boundary. All the specimens that fractured with the appearance of intergranular fracture had grain boundaries nominally ninety degrees to the loading axis. It is possible that the combination of large grains and random crystal orientation with each other and with respect to the tensile axis could have contributed to significant variation in life.

5. CONCLUSIONS

Review has shown that bulk pure Re in its various forms have been studied enough to develop some understanding of its deformation mechanisms and properties. Literature about pure LAM Re or any AM deposited Re is very limited. This work and others indicate LAM Re has some attractive mechanical properties such as better elevated temperature ductility but some properties such as strength are low. Fracture mechanisms most definitely vary with temperature. This work indicates a shear fracture mechanism not previously described in the literature for Re may be dominant at ultra-high temperatures. Fatigue fracture mode appears to depend on grain orientation with respect to tensile stress direction with two distinct modes appearing, intergranular and planar separation. Work to date has created information that begins to fill in some gaps in the open literature for LAM Re fracture but significant work remains to confirm the trends.

Results indicate that nanoindentation can determine selected mechanical properties for LAM Re. OIM has effectively characterized LAM Re crystal structure and enabled calculation of Young's modulus. However careful surface preparation is essential to properly use this tool.

There is some possibility of improved properties for Re alloys but very little work has been found in the literature.

6. FUTURE WORK

Many potential areas of inquiry have opened as a result of the work done in this program. Investigation into the effect of pure LAM Re grain size on strength could show a way to increase strength but perhaps maintain much higher ductility than found in Re fabricated from other methods of processing. Investigation of the existence and effect of twins at nanoindentation sites could shed light on deformation mechanism of Re, especially thin depositions. Alloying affects on LAM Re in conjunction with grain size reduction could also improve properties. Finally, fracture of LAM Re at ultra-high temperatures shows an unusual fracture feature, a relatively smooth surface. Investigation of this phenomenon could shed light on deformation mechanisms at these very high temperatures.

Perform additional study of the mechanism of fatigue initiation and propagation at room and elevated temperature. Fatigue in LAM Re appears to initiate at grain boundaries.

Finally coatings of Re should be characterized to enable commercial use of Re in the most efficient manner.

REFERENCES

1. Diaz, J. J., "Pure Rhenium Metal," *IEEE Potentials* (February/March 1996): 37-39.

2. Rabinowitz, E., "Friction and Wear Properties of Rhenium," *Wear* 10 (1967): 313-318.

3. Sherman, A. J., Tuffias, R. H., Kaplan, R. B., "The Properties and Applications of Rhenium Produced by CVD," *JOM* (July 1991): 20-23.

4. Sims, C. T., Wyler, E. N., Gaines, G. B., Rosenbaum, D. M., "A Survey of the Literature on Rhenium," Wright Air Force Development Center Technical Report 56-319, ASTIA Document No. AD 110596 (June 1956).

5. Bryskin, B., "Evaluation of Properties and Special Features for High-Temperature Application of Rhenium," *American Institute of Physics, Conf. 920104*, 246.1 (Jan. 15, 1992): 278-291.

6. Carlen, J-C., Bryskin, B. D., "Rhenium – A Unique Rare Metal," *Materials and Manufacturing Processes*, 9.6 (1994): 1087-1104.

7. Naor, A., Eliz, N., Gileadi, E., Taylor, S. R., "Properties and Applications of Rhenium and Its Alloys," The *AMMTIAC Quarterly*, 5.1 (2010): 11-15.

8. Polyak, D. E., "Rhenium," *U.S. Geological Survey, Mineral Commodity Summaries* (January 2010): 130-131.

9. Churchman, A. T., "Deformation Mechanisms and Work Hardening in Rhenium," *Transactions of the Metallurgical Society of AIME*, 218 (1960): 262-267.

10. Adams, R. J. and Mittendorf, D., Honeywell Chemical Metallurgical Reports 46442 and 56924 (2002).

11. Fengler, W. H., U.S. Patent Number 4048382 (Sept. 13, 1977).

12. Rabinowitz, E., *Friction and Wear of Materials* (New York: John Wiley and Sons, Inc., 1965).

13. Murphree, K., Shchetkovskiy, A., McKechnie, T., "High Temperature Bond and Thermal Barrier Coatings," *University Turbine Systems Research Workshop, State College, PA* (Oct. 19-21, 2010).

14. Hickman, R. R., McKechnie, T. N., Agarwal, A., "Net Shape Fabrication of High Temperature Materials for Rocket Engine Components," *37th AIAA/ASME/SAE/ASEE/ Joint Propulsion Conference, Salt Lake City, Utah* (July 8-11, 2001).

15. Singh, J., and Wolfe, D., "Nano-Grained Net-Shaped Fabrication of Re Components by EB-PVD," *Materials and Manufacturing Processes* 18.6 (2003): 915-927.

16. Singh, J,. and Wolfe, D., "Net-Shape Rhenium Fabrication by EB-PVD," *Advanced Materials and Processes* (April 2002): 39-42.

17. Arcella, F. G., Abbott, D., Cooper K. P. and Jones, H. N. "Laser Forming of Rhenium Near Net Shapes," *ASM AeroMet Conference, Orlando, Florida* (June 11-13, 2002).

18. Arcella, F. G., Abbott, D. H., Leonhardt, T., Cooper, K. P., "Properties of Laser Additive Manufacture (LAM^{SM}) Rhenium Tungsten Alloy Structures," *Structural Materials Division Conference, Rhenium Containing Alloys, New Orleans, LA* (Sept. 28, 2004).

19. Adams, R. J., "Ion Formation: An Alternative Additive Manufacturing Approach" *SAE Aerospace Manufacturing and Automated Fastening (AMAF) Conference, North Charleston, SC* (Sept. 18, 2008).

20. Leonhardt, T., Hamister, M., and Carlen, J-C., Biaglow, J., Reed, B., "Near-Net Shape Powder Metallurgy Rhenium Thruster," *36th Joint Propulsion Conference, Huntsville, AL,* NASA/TM-2001-210373 (July 17-19, 2000).

21. Bryskin, B. D., Diaz, D., "Metallography and Characterization of Rhenium and Rhenium Bearing Alloys," *Properties of Emerging P/M Materials, Advances in Powder Metallurgy and Particulate Materials,* 8 (1992): 183-197.

22. Schuster, G. B. A., "Grain Size Control of Rhenium Strip," *Eighth Symposium on Space Nuclear Power Systems, Albuquerque, NM* (Jan. 6-10 1991).

23. Leonhardt, T., Ritzert, F., "Prototype Rhenium Component for Stirling Engine Power Conversion," CP746, *Space Technology and Applications International Forum* (2005): 853-858.

24. Mittendorf, D., West, G. A., "New Processes to Produce Rhenium Metal Shapes," *Materials Manufacturing Processes,* 13.5 (1998): 749-755.

25. Schneider, S. J., "High Temperature Thruster Technology for Spacecraft Propulsion," *Acta Astronautica,* 28 (1992): 115-125.

26. Koeppel, R.J., Subhash, G., "Influence of Cold Rolling and Strain Rate on Plastic Response of Powder Metallurgy and Chemical Vapor Deposition Rhenium," *Metallurgical and Materials Transaction* 30 A (Oct. 1999): 2641-2648.

27. Carlen, J-C. and Bryskin, B., D., "Cold Forming Mechanisms and Work Hardening Rate for Rhenium," *Proceedings for the 13th International Plansee Seminar, Bildenstein, H. and Eck, R., ed., Metallwerk Plansee, Reutte,* 1 (1993): 79-90.

28. Koeppel, B. and Subhash, G. "Constitutive Response and Characterization of Deformation Modes in Rhenium," *Proceedings of the 2nd International Conference on Tungsten and Refractory Metals* (Princeton: Metal Powder Industries Federation, 1994): 673-680.

29. Koeppel, B. J., Subhash, G., "Plastic Response and Deformation Microstructure in Rhenium," *Microhardening Modeling and Damage Characterization of Advanced Materials* ASME AMD 199/MD 55 (1995): 93-100.

30. Private conversation with Lowell Munson of Honeywell (Sept. 2006).

31. Biaglow, J. A., "Rhenium Material Properties," *31st AIAA/ASME/SAE/ASEE Joint Propulsion Conference and Exhibit* San Diego, CA (July 10-12, 1995).

32. Chazen, M., L., "Materials Property Test Results of Rhenium," 31st *AIAA/ASME/SAE/ASEE Joint Propulsion Conference and Exhibit* San Diego, CA (July 10-12, 1995).

33. Dieter, G. E., *Mechanical Metallurgy* (Boston: McGraw-Hill, 1986).

34. Reed-Hill, R. E., Abbaschian, R. *Physical Metallurgy* (Boston: D.Van Nostrand Co., 1994).

35. Meyers, M.A. , Chawla, K. K., *Mechanical Behavior of Materials* (Upper Saddle River, NJ: Prentice Hall, 1999).

36. Greach, G. A., Jeffrey, R. A. and Smith, E. "The Deformation Characteristics in Rhenium Single Crystals," Gonser, B. W. ed. *Rhenium* (Amsterdam: Elsevier, 1962): 84-97.

37. Kopetskiy, CH. V., Myshlyayev, M. M., Novokhatskaya, N. I., Yukhanov, V. A. "Investigation of the Plastic Deformation of Rhenium Single Crystals," *Fiz. metal. metalloved.*, 39.1 (1975): 164-174.

38. Savitskii, E. M., Tylkina, M. A., Povarona, K. B., *Rhenium Alloys* (Jerusalem: Israel Program for Scientific Translations, 1970).

39. Larikov, L., Belyakova, M., and Rafalovski, V., "Structural and Density Changes of Rhenium Single Crystals Upon Rolling and Annealing," *Cryst. Res. Tech*., 26.2 (Feb. 1991): 239-244.

40. Jeffery, R. A., and Smith, E., "Deformation Twinning in Rhenium Single Crystals," *Phil. Mag.*, 13.126 (1966): 1163-1168.

41. Lageroloff, K. P., Xiao, S-Q., Bryskin, B. and Carlen, J-C., "Deformation Twinning of Rhenium," M.H. Yoo and Wuttig, M. ed. *Twinning in Advanced Materials* (The Minerals, Metals and Materials Society, 1994): 475-482.

42. Papirov, I. I., and Kapcherin, A. S., “Microhardness Anomalies of Rhenium,” *Fiz. metal. metalloved*., 51.3 (1981): 624-630.

43. Robinson, A. C., Zhang, X. J., L’Heureux, B. P., Gaies, J. G., “A Study on the Tensile and Fracture Toughness Behavior of Pure Rhenium Metal,” NSWCCD-61-TR-2006/0,1 (West Bethesda, MD: Naval Surface Warfare Center, Carderock Division, Feb. 2006).

44. Stephens, J. R., Witzke, W., R. “Alloy Softening in Group VIA Metals Alloyed with Rhenium,” NASA Report NASA TN D-7000 (Cleveland: Lewis Research Center, Nov. 1970).

45. Noddack,W., Tacke, I., Berg, O. “Eka-manganese: I. Chemical; II. X-Ray Part,” *Naturwissenschaften*, 13 (1925): 567-71.

46. Noddack,W., Tacke, I., “Rhenium and Masurium,” *Oersterr. Chem.-Ztg*., 28 (1925): 127-30.

47. *Personal Interview*, Melaven, D.A., Sims, C. T., Wyler, E. N., Gaines, G. B., Rosenbaum, D. M., “A Survey of the Literature on Rhenium,” Wright Air Force Development Center Technical Report 56-319, ASTIA Document No. AD 110596 (June 1956).

48. Fink, C. G., and Deren, P. “Rhenium Plating,” *Bull. Amer. Electrochem. Soc*., 66 (1934): 381-84.

49. Druce, J. *Rhenium* (Cambridge: University Press: 1948): 12-15.

50. Netherton, L., and Holt, M., “Electrodepostion of Rhenium from Aqueous Solutions,” *J. Electrochem. Soc*., 95 (1949): 324-328.

51. Schuth, W., and Klemm, W., “Magnetochemical Investigations: XI. The Magnetic Behavior of Some Rhenium Compounds,” *Z. anorg. allgem. Chem*., 220 (1973): 220-22.

52. Jaeger, F., and Rosenbohm, E., “Exact Measurement of the Specific Heats of Metals at Higher Temperatures: XII. Specific Heat of Metallic Rhenium,” *Proc. Acad. Sci. Amsterdam*, 36 (1933): 786-88.

53. Agte, C., Altherthum, H., Becker, K., Heyne, G., and Moers, K., “Physical and Chemical Properties of Rhenium,” *Z. anorg. allgem. Chem*., 196 (1931): 129-59.

54. Agte, C., Altherthum, H., Becker, K., Heyne, G., and Moers, K., “Physical Properties of Rhenium,” *Naturwissenschaften*, 19 (1931): 108-109.

55. “Investigations of Rhenium,” Wright Air Development Center TR 54-371, Battelle Memorial Institute to Aeronautical Research Laboratory, Wright- Patterson Air Force Base, Ohio (June 1954).

56. Sims, C., Craighead, C., and Jaffe, R., "Physical and Mechanical Properties of Rhenium," *Journal of Metals*, 8.1 (Jan. 1956): 168-179.

57. Lide, D. R., Fredderike, H. P. R., *CRC Handbook of Chemistry and Physics* (Boca Raton, FL: CRC Press, 1994): 12-37.

58. "Crystallographic Orientation," EDAX^{TSL} Advanced Microanalysis Solutions AMETEK.

59. Oliver, W. C. and Pharr G. M., "Measurement of Hardness and Elastic Modulus by Instrument Indentation: Advances in Understanding and Refinements to Methodology," *J. Mater. Res*., 19.1 (Jan. 2004): 3-20.

60. *The Nano Indenter XP System Manual*, MTS Systems Corporation (1999- 2002).

61. Gerd, S-N., Stixrude, L., Cohen, R. E. "First-Principles Elastic Constants for the hcp Transition Metals Fe, Co, and Re at High Pressure*," Physical Review B*, 60.2 (1 July 1999): 791-799.

62. Phillippe, L., Peyrot, I., Michler, J., Hassel, A. W., Milenkovic, S., "Yield Stress of Monocrystalline Rhenium Nanowires," *Applied Physics Letters*, 91, 111919 (2007).

63. Shepard, M. L. and Smith, J. F. "Elastic Constants of Re Single Crystals in the Temperature Range 4.2-298 K," *Journal of Applied Physics* 36.4 (Apr. 1965): 1447-1450.

64. The International Union of Crystallography, *International Table for X-ray Crystallography* (Birmingham: The Kynoch Press, 1959): 112 -115.

65. Nye, J. F. *Physical Properties of Crystals* (Oxford: Oxford University Press, 1957): 143-149.

66. Suresh, S., *Fatigue of Materials* (Cambridge: Cambridge University Press, 1998).

67. Leonhardt , T. "Advanced Powder Metallurgical Techniques for Spherical Rhenium Metal Powder" BMDO SBIR Phase II, Contract number N00167-02-C-0067, Line Item number 0001AP.

68. Adams, R. J. , Giesler, W., Langston, "Wear and Oxidation Resistant Rhenium Alloys" *ASM AeroMat 2005 Conference*, (Orlando, Fla. June 6-9, 2005).

69. *Tungsten,* Schwarzkopf Development Center, Plansee SE.

APPENDIX A

Re TENSILE TOOLING CALCULATIONS

Furnace

A Thermal Tech vacuum furnace with tensile and compression loading capability was used at Honeywell. Load, displacement and control were manufactured by MTS.

Arrangement

W load tooling arms in high temperature zone is attached to INCONEL couplings and alignment adjustment which in turn is attached to the furnace loading arms.

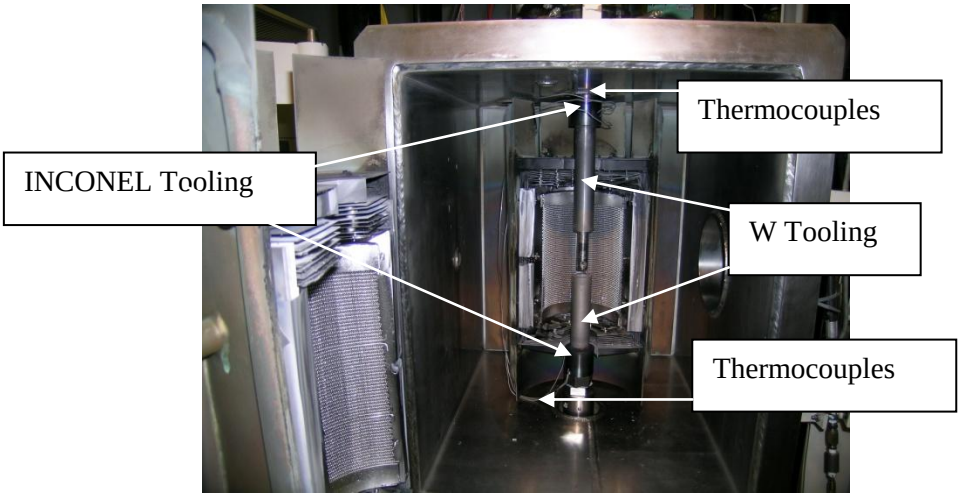

The first task is to verify that the W and INCONEL tooling are dimensioned sufficiently for the loads anticipated.

At 1925 °C W has a strength of ~ 100 N/mm^2 (14,500 psi)[1].

At 871 °C W has a strength of ~ 750 N/mm^2 (105,000 psi)[1].

At room temperature the ductile-to-brittle of W varies between 90 °C and 450 °C[2].

At 871 °C INCONEL 718 has a tensile strength of ~ 276 MPa (40,000 psi)[3]

Loading

From previous tests the stress could reach as high as ~ 90 MPa (13 ksi) or as low as 62 MPa (9 ksi). To be conservative assume the maximum stress is 172 MPa (25 ksi). The

area of the specimen to be tested is 0.080" thick by 0.125" wide. The load is then Load = area*stress =.080"*.125" * 25,000 = (.010 in.sq.^2)* 25,000 = 300 lbs = 1334 N

Pin Bending

The stress in the pin from bending = Moment/Section modulus = Ft/(I/c)

Where M= F*t and F= the shearing force and t = grip of the rivet i.e. the thickness of the connected parts[3]. Assume 2 grip scenario's i.e.

1. grip = coupling wall thickness =.450" thick and
2. grip = 2*coupling wall thickness + W load arm = 2*.450 + 1.5" = 2.4" = t

Therefore for case 1. $M_1 = F*t_1$ = 300 lbs *.450" = 135 in-lb

And for case 2. $M_2 = F*t_2$ = 300*2.4 = 720 in-lb

For all cases I= $pi*R^4/4 = pi(.375)^4/4$ = 3.1416(.0198)/4 =.016 in^4

Thus stress 1 = S_1 = 135/((.016)/(.375/2)) = 135/(.016/.1875) = 135/.0853 = 1582 psi (10.9 MPa)

For stress 2 = S_2 = 720/((.016)/(.375/2)) = 720/.0853 = 8441 psi (58.2 MPa)

Shear Stress in Pins and W Load Arm Due to Pin Loading

W loading arms hold specimen with two collets sandwiching the specimens. They are intended to reduce the bending on the W pins that hold the specimen and collets in place. The collets and specimen have three 0.100" holes in an upside down triangle that pass through the W tooling, the collets and specimen to hold the specimen in place and apply the load. Thus the total load exerted on the arm is passed through the load arms to the specimen via 6 tungsten rods approximately 0.094" in diameter. Thus the load in each hole is 1/6 the total load exerted on the arm. The W annulus wall is 0.3" thick.

Since three pins acting through 6 holes carries 300 lbs, each hole will bear 50 lbs.

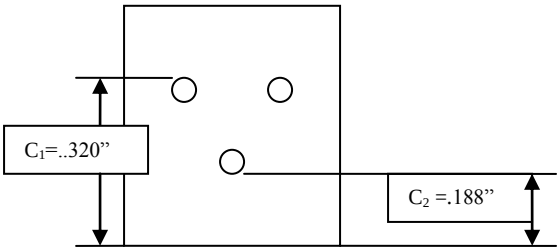

Distances are from hole centerline

Sample pin in W load/colette arm shear stress

Pin shear stress = S_{pin} = Load/shear area i.e. x-sectional area of pin = load/2*C*a =

50/(pi(.094^2/4)) = 50/.007 = 7205 psi (49.7 MPa)

Actual loads are (70/6)/.007 = 11.6/.007 = 1657 psi (11.4 MPa)

Coupling pin shear stress

Coupling pin shear stress = S_{pinc} = Load/shear area i.e. x-sectional area of pin =

150/(pi(.375^2/4)) = 150/.11 = 1364 psi (9.4 MPa)

Shear Loading in W tooling at pins

S_s = f/(2*c_{i*}a) where c is the distance from the end of the tooling arm to the hole center-line and $a_{tooling}$ = W tooling wall thickness = a_t =.3

S_s = f/(2*c_{i*}a) = 50/(2*.320*.3) = 781 psi (5.4 MP)

S_s = f/(2*c_{i*}a) = 50/(2*.188*.3) = 443 psi (3.05 MPa)

Compression stress 2 each hole due to pin pressure

S_c = f/(2*d_*a) = 50/(2*.100*.3) = 833 psi (5.7 Mpa)

W Load Arm nominal tensile stress away from pin:

Load arm is 1.5” in diameter = b, therefore the area is Pi*(1.5^2/4) = 1.77 sq.in

x-sectional area Stress = F/A = S_{arm} = 300/1.77 = 169 psi (1.2 MPa)

W Load Arm Nominal Tensile Stress at Pin

Load arm is 1.5” in diameter = b, therefore the area is Pi*(1.5^2/4) = 1.77 sq.in

$A_{pin/load\ arm}$ = Load arm area – maximum pin area = 1.77 sq.in -.375(1.5) = 1.77-.562

$A_{pin/load\ arm}$ = 1.208 sq.in.

Stress = load /area = 300 lbs/1.208 sq.in. = 248 psi (1.7 MPa)

Stress in INCONEL Coupling due to Tensile Load (Coupling has 0.37 dia. Pin Transverse to Coupling Axis)

$a_{coupling} = a_c$ = coupling wall thickness =.450 inch (11.4 mm)

D = coupling diameter = 2.3 inch (58.4 mm)

Tensile stress = S_t = load/(wall thickness area – pin dia. area) = F/(pi*($D^2 – b^2$)) =

300/(3.1416*((2.3^2/4) – (1.5^2/4)) -.375*.450) psi = 300/(3.1416*(1.32 -.563) -.169))

S_t = 300/2.21 = 136 psi (.938 MPa)

Tensile Loading in Arm in W Annulus for Collets

A_{arm} = area of annulus = pi(D^2/ 4– d^2/4) = 3.1416(1.5^2/4 -$.9^2$/4) = pi(.56 -.2) = 1.131 in sq

(730 mm^2)

Tensile stress = F/A = 300/1.131 = 265 psi (1.83 MPa)

Assume k_t= 3 at each hole then stress at each hole is 38 265 = 795 psi (5.48 MPa)

Rough final specimen measurement while still in tooling

.4+.350 =.750 (.750 -.5)/.5 =.25/.5 =.50, 50 percent

Preliminary Estimated stress from P6 tests

<u>As-deposited Re:</u> Stress = Load/area = 70/(.080”*.125”) = 70/(.010 in.sq.^2) = 7000 psi

(48.3 MPa)

<u>Rolled and annealed Re:</u> Stress = Load/area = 158/(.080”*.125”) = 158/(.010 in.sq.^2) =

15,400 psi (106 MPa)

RA Re elongation

Original length of specimen 1 = 2.006 inch (50.1 mm), Final length = 2.1337 (54.2 mm), effective gauge length from previous two tests = 0.063 per ASTM 21

Assume all elongation is in effective gauge length and visually it appeared so

Lo –Lf =.1337 but let's assume 0.1 = 2.54 mm because the specimen had a small gap between the fracture faces in order to keep the fracture features damage free.

Elong. = $(L_{oeff\ fin} - L_{oeff})/L_{oeff}$ =.1/.063 = 0.159, therefore elongation is ~ 15.8 percent

Fracture Mechanics Assessment of nicks near W tooling pin holes:

The brittle transition temperature of W varies from ~ 100 °C to 400 °C depending on manufacturing process and annealing temperature.[69] K_{Ic} varies from ~ 100 psi $(in)^{1/2}$ to 200 psi $(in)^{1/2}$, Tensile strength =yield strength = 242 to 297 ksi (1669 to 2048 MPa)

Let W load arm tensile annulus stress = σ then

$K_{Ic} = 1.1(\pi)^{1/2}M_K(\sigma)\ (a/Q)^{1/2}$

Where K_{Ic} is the fracture toughness, pi = π = 3.1416, M_K = magnification factor and is proportional to a/t, Q= flaw shape parameter and is proportional to a/2c and the nominal stress = σ = 265 psi (1.83 MPa).

Let t =.3" then assume a =.1 and a/t =.1/.5 =.5 therefore from figure 5.11 from Rolfe M_K = 1.

Let a/2c =.5 then Q is dependent on the ratio of $\sigma = \sigma_y$ = yield stress ~ tensile stress = 242 ksi ~ negligible. Thus from Fig. 5.12 p. 159, Q = 2.5.

Solve for a.

$(a/Q)^{1/2} = K_{Ic} / (1.1(\pi)^{1/2}M_K(\sigma)) = 100\ psi(in)^{1/2} / 1.1(3.1416)^{1/2}(1)(265\ psi)$

$(a/Q)^{1/2} = 100/1.1(1.772)(1)265 = .19$

$(a/Q)^{1/2} = (a/2.5)^{1/2} = (.4a)^{1/2} = .19$

.4a =.0375

a =.0937 in = 2.378 mm = largest crack allowable below ductile-to-brittle transition temperature (DBTT) at a load of 265 psi (1.83 MPa).